https://doi.org/10.5194/egusphere-2023-182
Preprint. Discussion started: 29 March 2023

O_3 and PAN in southern Tibetan Plateau determined by distinct physical and chemical processes

Wanyun Xu[1], Yuxuan Bian[1], Weili Lin[2], Yingjie Zhang[3,a], Yaru Wang[3,b], Gen Zhang[1,*], Chunxiang Ye[3,*] , Xiaobin Xu[1]

[1] State Key Laboratory of Severe Weather & Key Laboratory for Atmospheric Chemistry of CMA, Institute of Atmospheric Composition, Chinese Academy of Meteorological Sciences, Beijing, 100081, China
[2] College of Life and Environmental Sciences, Minzu University of China, Beijing, 100081, China
[3] College of Environment, Peking University of China, Beijing, 100871, China
[a] now at School of Ecology and Nature Conservation, Beijing Forestry University, Beijing, 100083, China
[b] now at Leibniz Institute for Tropospheric Research, 04318 Leipzig, Germany

Correspondence to: Gen Zhang (zhanggen@cma.gov.cn) and Chunxiang Ye (c.ye@pku.edu.cn)

Abstract. Tropospheric ozone (O_3) and peroxyacetyl nitrate (PAN) are both photochemical pollutants harmful to the ecological environment and human health. In this study, measurements of O_3 and PAN as well as their precursors were conducted from May to July 2019 at Nam Co station (NMC), a highly pristine high-altitude site in the southern Tibetan Plateau (TP), to investigate how distinct transport processes and photochemistry contributed to their variations. Results revealed that, despite highly similar diurnal variations with steep morning rises and flat daytime plateaus that were caused by boundary layer development and downmixing of free tropospheric air, day to day variations in O_3 and PAN were in fact controlled by distinct physiochemical processes. During the dry spring season, airmasses rich in O_3 were associated with high altitude westerly airmasses that entered the TP from the west or the south, which frequently carried high loadings of stratospheric O_3 to NMC. During the summer monsoon season, a northward shift of the subtropical jet stream shifted the stratospheric downward entrainment pathway also to the north, leading to direct stratospheric O_3 entrainment into the troposphere of the northern TP, which travelled southwards to NMC within low altitudes via northerly winds in front of ridges or closed high pressures over the TP. Westerly and southerly airmasses, however, revealed low O_3 levels due to the overall less stratospheric O_3 within the troposphere of low latitude regions. PAN, however, was only rich in westerly or southerly airmasses that crossed over polluted regions such as Northern India, Nepal or Bangladesh before entering the TP and arriving at NMC from the south during both spring and summer. Overall, the O_3 level at NMC was mostly determined by stratosphere-troposphere exchange (STE), which explained 77% and 88% of the observed O_3 concentration in spring and summer, respectively. However, only 0.1% of the springtime day-to-day O_3 variability could by STE processes, while 22% was explained during summertime. Positive net photochemical formation was estimated for both O_3 and PAN based on observation-constrained box modelling. Near surface photochemical formation could not explain the high O_3 level observed at NMC and was also not the factor determining the day-to-day variability of O_3, however, it captured events with elevated PAN concentrations and was able to explain its diurnal variations. Both O_3 and PAN formation were highly sensitive to NO_x levels, with PAN being also quite sensitive to VOCs concentrations. Under the rapid development of transportation network

https://doi.org/10.5194/egusphere-2023-182
Preprint. Discussion started: 29 March 2023

and the urbanization inside the TP, increased emissions and loadings in NO_x and VOCs might lead to strongly enhanced O_3 and PAN formation in downwind pristine regions, which should be paid more attention in the future.

1 Introduction

Ozone (O_3) and peroxyacetyl nitrate (PAN) are both key photochemical pollutants within the troposphere, that are harmful to vegetation and human health (Kleindienst et al., 1990;Yukihiro et al., 2012;Taylor, 1969;Lefohn et al., 2017). Since O_3 and PAN are both produced during the oxidation of volatile organic compounds (VOCs) in the presence of nitrogen oxides (NO_x), they often share highly similar variational characteristics (Fischer et al., 2014). However, PAN is formed only from a limited number of oxygenated VOCs (OVOCs), which are typically oxidation products of alkenes (with low carbon numbers), aromatics and isoprene (Xu et al., 2021), while O_3 can be practically formed from all VOCs. Additionally, the photochemical formation of O_3 depends highly nonlinearly on its precursor concentrations, being insensitive to VOCs changes under NO_x-limited conditions and vice versa, while PAN varied nearly proportional to its OVOCs precursors, with additional influences from the NO_2 to NO ratio (Xu et al., 2021). Thus, photochemistry can sometimes result in distinct variations of O_3 and PAN, especially during cold seasons (Xu et al., 2021;Zhang et al., 2020). From the aspect of physical transport, O_3 and PAN can be both transported over large distances. Since PAN is easily thermal decomposed under high temperatures, its transport is more favored in cold seasons or at higher altitudes. Early simulation studies suggested PAN to be an important reservoir for NO_x in the troposphere and lower stratosphere (Singh and Hanst, 1981) and redistributes NO_x far from its source regions (Moxim et al., 1996). Different from PAN, O_3 is naturally produced within the stratosphere and can be transported into the troposphere via stratosphere-troposphere exchange (STE) processes that are often associated with the occurrence of tropopause folds, cut-off lows, streamers near the polar-front jet and subtropical jet stream and mid-latitude cyclones (Langford, 1999;Stohl et al., 2003;Sprenger et al., 2007;Tang et al., 2011). STE elevates tropospheric O_3 and oxidation capacity at distinct latitudes during different seasons, with overall largest mass fluxes in summer occurring mostly in higher mid latitudes, followed by spring occurring mostly in lower mid latitudes (Tang et al., 2011;Škerlak et al., 2014). Deep STE intrusions reaching the planetary boundary layer (PBL) and associated mass fluxes are largest during spring in China and the western part of North America.

While the variational characteristics, influence of photochemical formation and transport on O_3 and PAN have been widely investigated in polluted urban regions of China (Liu et al., 2018;Yao et al., 2019;Hu et al., 2020;Wei et al., 2020;Qiu et al., 2021;Zhang et al., 2021;Xu et al., 2021), those at remote background sites received less attention, especially for PAN. The Tibetan Plateau (TP), located in western China, is often called the “Third Pole” with its average altitude over 4000 m. Due to its harsh environment, the TP is only scarcely populated and thus highly pristine. The topography of the TP affects large scale circulations with its strong thermal forcing, thereby influencing the weather, climate and air quality in eastern China (Yang et al., 2014). Surface O_3 as a crucial greenhouse gas and with its deterministic role on atmospheric oxidation capacity

https://doi.org/10.5194/egusphere-2023-182
Preprint. Discussion started: 29 March 2023

has been paid certain attention in the TP and special concern has been paid to the photochemical formation of O_3 under the strong radiative conditions at such high altitudes. Ma et al. (2002) investigated the photochemical formation of O_3 at Mt. Waliguan (WLG) in the Northeastern TP through box-modelling and suggested wintertime net production and summertime net loss in O_3. Xue et al. (2013) further constrained the box model with VOCs sampling results, which mainly included hydrocarbons and aromatic compounds (no oxygenated compounds), and found net O_3 formation at WLG during both spring and summer 2003. Transport from central and eastern China was found to be frequent during summertime (Xue et al., 2011;Xu et al., 2018a), which revealed higher O_3 production efficiencies (Xue et al., 2011) and was responsible for rising O_3 trends during summer and autumn (Xu et al., 2016;Xu et al., 2018a). Due to its high altitude, the TP revealed the largest deep STE O_3 mass fluxes, with higher fluxes in spring and winter and lower ones in summer and autumn, especially in the southeastern TP (Škerlak et al., 2014). At WLG, O_3 was observed to be strongly influenced by STE associated with the subtropical jet during spring and summer in 2003, with stronger impacts during summer than spring (Ding and Wang, 2006;Zheng et al., 2008). STE was estimated to contribute an annual average of 10.2% to tropospheric O_3 at WLG based on EMAC model simulations using tagged tracers, revealing a peak contribution in June (Liu et al., 2020). At Nam Co station (NMC) in the southern TP stratospheric influence was also mainly observed during spring and summer, which was estimated to contribute 20% and 10%, respectively, based on model simulations (Yin et al., 2017). Measurements from Dangxiong, a lower site not far from NMC, also revealed significant stratospheric impacts on surface O_3 (Lin et al., 2015). At Xianggelila station in the southeastern TP, the STE impact was suggested to be most pronounced during winter and weakest during spring and summer based on surface observations (Ma et al., 2014), which however was in disagreement with modelling results revealing strongest STE during April and May, with an annual average contribution of 4.3%. In comparison, PAN was far less investigated, the few existing studies mainly focused on the impact of transport on local PAN variations. Zhang et al. (2009) made measurements of O_3 and PAN at WLG station during summer 2006 and found that the two oxidants exhibited distinct diurnal variations and only weak correlations to each other, suggesting they were controlled by different processes, with PAN being strongly influenced by regional transport of polluted air plumes. Xue et al. (2011) analyzed the same set of observations and reported PAN to be one of the most abundant reactive nitrogen species (NO_y) at WLG, contributing 32% to total NO_y. Xu et al. (2018b) made measurements of O_3 and PAN at NMC station in summer 2011 and late spring to early summer 2012, detecting highly similar diurnal variations in both gases caused by boundary layer development and elevated PAN in connection with transport of air plumes crossing over Nepal, North Pakistan or North India.

Despite the findings in previous literature, the physiochemical factors determining the variation of O_3 and PAN in the TP and their relative contributions have not been comprehensively investigated mainly due to the lack of comprehensive online VOCs observations and accurate NO_x measurements. In this study, we present integrated real-time measurements of O_3, PAN, NO_2, VOCs, CH_4, CO, photolysis rates and other meteorological parameters during spring and summer 2019 at NMC station and analyzed them in combination with reanalysis data, utilizing trajectory modelling and box-modelling approaches. The different impact of distinct transport processes and photochemical formation on O_3 and PAN, as well as

https://doi.org/10.5194/egusphere-2023-182
Preprint. Discussion started: 29 March 2023

differences in sensitivities towards their precursors are intercompared using improved box-model constraints and the relative contributions of physical and chemical processes to O_3 and PAN variability are evaluated.

2 Experimental and analysis methods

2.1 Site, observations and data

As the first part of the @Tibet series campaign, a campaign was carried out at NMC Station (30.77° N, 90. 95° E, 4730m a.s.l.), which is a highly pristine site in the southern TP (Fig. 1). The site campus is located within the natural reserve of NMC Lake, thus far away from anthropogenic activities and emissions. The nearest county (Dangxiong) and city (Lhasa) are located 40 and 125 km to the southeast of NMC, respectively. The NMC Lake was ~1 km north to our observation site, while the foothills of the northern Nyainqêntanglha Mountains were ~15 km to the south.

Measurements were performed from 1 May to 31 July 2019. Instruments for gases (including O_3, PAN, NO_2, CO, CH_4 and non-methane volatile organic compounds (NMVOCs)) were housed in an air-conditioned container. O_3 was measured alternatingly at the heights of 1.8 and 6.8 m (switching between two heights at 15-minute intervals) using a Model TE-49C commercial O_3 analyzer, which was calibrated with a TE-49iPS O_3 calibrator (both from Thermo Electronics, USA). A Los Gatos Research (LGR) NO_2 Analyzer was adopted for the measurements of NO_2, which has a measurement range of 0.01-1000 ppb and was calibrated using NO_2 standard gas at the beginning and end of the experiment. PAN measurements were made using a GC-ECD analyzer (Meteorologie Consult GmbH, Germany) which was calibrated using PAN instantly formed in the reaction of a NO reference gas with acetone in the internal calibration unit of the instrument. CO and CH_4 were measured (until 2 July) by a cavity ring-down spectroscopy (CRDS) analyzer (Model G2401, PICARRO, USA) at a high precision (0.4 and 0.04 ppb, respectively, for CO and CH_4). The CRDS instrument was calibrated twice using a mixed CO and CH_4 standard gas, which was pressurized in 29.5 L treated aluminum alloy cylinders (Scott-Marrin Inc.) fitted with high-purity, two-stage gas regulators, and calibrated with cylinders assigned by the Global Atmosphere Watch (GAW) CO Central Calibration Laboratory operated by National Oceanic and Atmospheric Administration (NOAA) Earth System Research Laboratory (ESRL). NMVOCs were measured (only from 29 April to 21 May) using an online GC-MS/FID analysis system (TH-PKU 300B, Wuhan Tianhong Instrument Co. Ltd., China) at a 1-hour time resolution, with detection limits in the range of 0.004 to 0.066 ppb. Multipoint calibrations were performed using Photochemical Assessment Monitoring Stations (PAMS) standard mixture and TO-15 standard mixture (100 ppb, Spectra Gases Inc., New Jersey, USA). To account for the reactivity of different VOCs species, Propy-Equivalent VOCs concentrations were calculated as:

$$C_{Propy-Equiv}(i) = C(i)\frac{k_{OH}(i)}{k_{OH}(C_3H_6)}, \quad \text{Eq. (1)}$$

where C(i) is the ppbC concentration of species *i* (calculated using ppb mixing ratios multiplied by carbon numbers of species *i*), $k_{OH}(i)$ the reaction rate of species *i* with OH radicals (obtained from master chemical mechanism, http://mcm.york.ac.uk/MCM/), and $k_{OH}(C_3H_6)$ the reaction rate of propene with OH.

https://doi.org/10.5194/egusphere-2023-182
Preprint. Discussion started: 29 March 2023

Photolysis rates (J values) were obtained using a Metcon CCD-spectrograph (Meteorologie consult GmbH, Germany), whose receptor optics were mounted on top of the container at the height of 2 m. Conventional meteorological parameters including temperature (T), relative humidity (RH), surface pressure (P), wind speed (WS) and wind direction (WD) were recorded by an Automatic Weather Station. In addition, meteorological reanalysis data (ERA5) from the European Centre for Medium-Range Weather Forecasts (ECMWF) were used for complimentary analysis.

2.2 Backward trajectory analysis and PSCF calculations

The HYSPLIT model (version 5) from NOAA Air Resources Laboratory (Draxler and Hess, 1997;Draxler and Hess, 1998;Draxler, 1999) was used for backward trajectory calculations, with 0.25° resolution GFS data from the National Center for Environmental Prediction (NCEP) adopted as input. The trajectory endpoint was set at 250 m above the ground level of NMC station. 7- day (168 hours) backward trajectories were calculated at an hourly interval for the entire period of the campaign.

The potential sources of high O_3 and PAN were studied using the potential source contribution function (PSCF) analysis, which has been widely applied to detect possible source regions (Ara Begum et al., 2005;Lucey et al., 2001;Zhou et al., 2004). The PSCF on grid (i,j) is defined as:

$$PSCF = m(i,j)/n(i,j), \quad (1)$$

where m(i,j) is the residence time of a subset of trajectories, whereas n(i,j) is the residence time of all the trajectories in that grid. Each trajectory was associated with O_3 and PAN concentrations observed at its time of arrival. To pin out the potential source regions for high O_3 and PAN, the m(i,j) was calculated using the subset of trajectories that were associated with O_3 or PAN concentrations higher than their respective 75th percentiles.

Abnormally high PSCF values may be produced for certain grids with very small n(i,j) values, which would induce large uncertainties. Thus, a weighting factor W(n_{ij}) is introduced that was proposed by Zeng and Hopke (1989), giving grids with few trajectories passing through less weight:

$$W(n_{ij}) = \begin{cases} 1.0, & n_{ij} > \overline{n_{ij}} \\ 0.7, & 0.1 \cdot \overline{n_{ij}} < n_{ij} \le \overline{n_{ij}} \\ 0.4, & 0.05 \cdot \overline{n_{ij}} < n_{ij} \le 0.1 \cdot \overline{n_{ij}} \\ 0.2, & n_{ij} \ge 0.05 \cdot \overline{n_{ij}} \end{cases}, \quad (2)$$

where $\overline{n_{ij}}$ is the average number of n_{ij}.

The PSCF analysis was respectively performed for O_3 and PAN, separately for spring and summer periods. Based on meteorological variations, spring and summer periods were defined as 1 May to 15 June and 15 June to 31 July, respectively.

https://doi.org/10.5194/egusphere-2023-182
Preprint. Discussion started: 29 March 2023

2.3 Box modelling of local photochemistry

The Master Chemical Mechanism (version 3.2) was used within the F0AM (version 3.1) box-model framework developed by Wolfe et al. (2016), to simulate the impacts of local photochemistry on O_3 and PAN and to evaluate how much of their variations can be explained through local photochemistry. Observation data of VOCs, NO_2, J values and meteorological parameters were either averaged or interpolated into 10-minute averages and used as constraints in the model. Model simulations were only performed for the period from 1 to 21 May, when VOCs observation data were available. To evaluate local O_3 and PAN formation, three sets of simulations were performed for each, respectively using measurement constraints on OVOCs, NO_2 or both of them. In O_3 simulation cases, PAN was constrained by observations, while in PAN simulations O_3 was constrained. Daytime O_3 and PAN increments ($\Delta O_{3,mod}$ and ΔPAN_{mod}) were calculated and compared against observed ones ($\Delta O_{3,obs}$ and ΔPAN_{obs}), with their ratios used to reflect how much modelled local photochemistry can explain observed daytime increases in O_3 and PAN. Simulated O_3 and PAN net formation rates in distinct modelling scenarios were intercompared and to evaluated the sensitivity of their formation to VOCs and NO_x concentrations.

2.4 Impact of stratospheric-tropospheric exchange

A Y index was defined as the ratio between normalized O_3 and water vapor concentrations, calculated using the following equation:

$$Y_{ind} = \frac{O_3/\overline{O_3}}{H_2O/\overline{H_2O}}. \quad \text{Eq. (3)}$$

The Y index adopted in previous studies for the identification of stratospheric air intrusions has additionally divided Eq. (3) by normalized CO concentrations (Ma et al., 2014). Due to the lack of CO measurements after 2 July, the Y index was modified to the current form (in Eq. 3), which compared well with those calculated when incorporating normalized CO concentrations (Fig. S1), since CO revealed very small variability during the entire observation period.

Additionally, O_3 mass mixing ratios from the ERA5 hourly reanalysis dataset were converted to volume mixing ratios and applied in the investigation of STE impacts, since the ERA5 data are simulated with simple stratospheric O_3 chemistry consideration and thus mainly represents the physical transport of stratospheric O_3 (Sprenger and Wernli, 2003). Additionally, ERA5 O_3 data has been verified to be well representative of observed O_3 profiles and ground concentration levels at remote polar regions (Wang et al., 2021), indicating that it can well represent stratospheric O_3 and the influence of its transport.

https://doi.org/10.5194/egusphere-2023-182
Preprint. Discussion started: 29 March 2023

3 Results and discussions

3.1 Variational characteristics of O3, PAN and their precursors

The time series of observed O_3, PAN, NO_2, CO, photolysis rates of O_3 (jO^1D) and NO_2 (jNO_2), as well as meteorological parameters observed at NMC from 1 May to 31 July are displayed in Figure 2. From 1 May to 15 June (defined hereafter as the spring period), NMC experienced cold temperatures, strong winds, and dry conditions with low relative humidity (RH) and hardly any precipitation except for three small snow events. While during 15 June to 31 July (defined hereafter as the summer period), temperatures increased, average wind speeds were smaller and frequent precipitation events occurred under the influence of the Asian summer monsoon (Fig. 2a, Table 1). Despite more frequent precipitation events, observed average daytime photolysis rates were similar between spring and summer periods.

Under such meteorological variations, O_3 and PAN exhibited higher average concentrations in the spring (59.8±13.4 and 0.27±0.08 ppb) and lower ones in the summer period (53.6±13.2 and 0.20±0.05 ppb), with O_3 levels being overall in accordance with previous observations (Xu et al., 2018b;Yin et al., 2017), while PAN levels were significantly lower than those observed in 2012 (Xu et al., 2018b). VOCs concentrations were only obtained for the first half of the spring period, reaching average concentrations of 4.1±3.5 Propy-Equiv. ppbC, to which OVOCs contributed 61±12% (reaching 2.5±2.2 Propy-Equiv. ppbC on average), followed by alkenes (0.6±0.6 Propy-Equiv. ppbC), aromatics (0.6±1.3 Propy-Equiv. ppbC) and alkanes (0.47±0.5 Propy-Equiv. ppbC), which made up similar fractions (14±6%, 13±7%, and 11±4%, respectively), while other components (including alkynes, halogenated VOCs and nitriles) had negligible impacts (1±1%) on the overall VOC concentration and reactivity (Fig. S2). While daytime concentrations of OVOCs and alkenes were significantly higher than those during nighttime, other VOCs species did not display much day-night discrepancy. NO_2 revealed averaged concentrations 0.12±0.05 and 0.09±0.05 ppb during spring and summer periods, respectively, with no evident day to night differences.

Averaged diurnal variations of O_3 and PAN resembled each other (Figs. 3a1-2), both revealing decreases after sunset, reaching lowest values at 7:00 Beijing Local Time (LT) and increasing quickly after sunrise simultaneous to PBL height (PBLH, Figs. 3b1-2) and exhibiting a flat plateau afterwards. Both O_3 and PAN revealed higher levels in spring and lower ones in summer, however, PAN concentrations have decreased more significantly than O_3 (26% versus 10%), revealing a very flat and broad plateau during the day. OVOCs, aromatics and alkenes determined the variations of VOCs, with OVOCs and alkenes displaying diel variations similar to those of O_3 and PAN, revealing increases from 7:00 to 9:00 LT, fluctuating around its daily maximum value over daytime and decreasing after 17:00 LT (Figs. 3b1-2). NO_2 was typically higher during nighttime and lower during daytime, which is caused by combined effects of weakened dilution under nighttime shallow boundary layers, natural and anthropogenic NO_x emissions, as well as chemical transformations. Additionally, springtime NO_2 concentrations were higher than those during the summer period (Figs. 3c1-2). CO, however, revealed only slightly higher concentrations during the summer period, staying overall flat during the day, without any diurnal variations (Figs. 3c1-2). Both RH and absolute water vapor concentrations were higher during the summer period. RH revealed a diurnal

https://doi.org/10.5194/egusphere-2023-182
Preprint. Discussion started: 29 March 2023

maximum by 7:00 LT during both periods, decreased rapidly after sunrise and reached its diurnal minimum at 16:00 and 18:00 LT in spring and summer, respectively (Fig. 3e1-2). Water vapor, however, increased further after sunrise, possibly due to surface evaporation processes of frost and dew during the morning. While the diurnal peak in photolysis rates were similar between spring and summer periods, the averaged diurnal variations displayed a narrower peak during summer, especially for jNO_2, due to more frequent precipitation and higher cloud coverage.

The day-to-day evolution of diurnal O_3 and PAN variations as well as those of winds and PBLH are more clearly displayed by Figs. 4). Downward winds were strongest during the afternoon under high PBLH (Figs. 4a,d). Due to the local topography with the NMC Lake to its west and north and the Nyainqêntanglha Mountains to its south, the site was susceptible to both influences from land-lake and mountain-valley breezes. Accordingly, local surface winds displayed clear diurnal variations with southeasterly nighttime winds shifting to northwesterly winds during daytime (Figs. S3b-d, Fig. S3 is the same as Fig. 4, with winds replaced by 2 m wind measurements). 550 hPa winds from ERA5 over the 0.25° grid containing NMC station (representing near surface conditions, since surface pressure was on average 573±2 hPa) revealed stronger diurnal variations in zonal winds (Fig. 4b), overall agreeing with variations in surface winds, while meridional winds were dominated by southerly wind directions (Fig. 4c), with occasional changes to northerly winds, suggesting that local circulations had stronger impacts on zonal winds.

Broad peaks in O_3 often lasted until late evening hours, while nighttime O_3 frequently revealed increases under westerly winds and could reach daytime concentration levels, which can only be attributed to transport processes. High nighttime O_3 was not always accompanied by simultaneous PAN increases, while vice versa, elevated nighttime PAN was also not always synchronized with those of O_3, indicating that they might have originated from distinct sources and processes. O_3 levels were continuously high throughout the spring period, especially during 6-13 May. Despite overall lower levels in the summer period, two O_3 episodes occurred during 7-8 July and 24-25 July, respectively, exhibiting the highest concentrations observed during the entire campaign (Fig. 2a, Fig. 4e). Compared to O_3, PAN displayed much larger day to day variability, with an evident high PAN episode occurring from 13 to 16 May under southeasterly winds from aloft (Fig. 4f). Summertime PAN was distinctly lower than that during spring season, with no increases detected during the two high O_3 episodes.

Overall, while O_3 and PAN revealed highly similar average diurnal variation patterns, their temporal variations often differed from each other, suggesting that they were determined by distinct transport or formation processes, which will be further investigated in the following sections.

3.2 Impact of local circulation

In previous studies, diurnal variations in O_3 and PAN were mainly attributed to local circulations, particularly the development of the PBL. At pristine mountain sites such as WLG, surface O_3 was influenced by free tropospheric air during nighttime and by boundary layer airmasses during daytime, which resulted in a diurnal cycle with lower daytime and higher nighttime O_3 with very small diurnal variation amplitudes. Despite its high altitudes, NMC is located at the foot of the northern Nyainqêntanglha Mountains, and thus experienced local circulation distinct from those at WLG. Free tropospheric

https://doi.org/10.5194/egusphere-2023-182
Preprint. Discussion started: 29 March 2023

air was suggested to be richer in O_3 and PAN concentrations and was mixed down upon the rapid development of the convective boundary layer (CBL) after sunrise, while O_3 and PAN concentrations decreased upon the establishment of the nocturnal boundary layer (NBL), due to the dominance of local boundary layer airmasses during nighttime, which were low in O_3 and PAN, since barely any surface O_3 and PAN precursor emission sources existed at NMC, added by effects of dry deposition (Xu et al., 2018b). The broad O_3 peaks that often lasted until late evenings and the frequent events of elevated nighttime O_3 (Fig. 4e) both supported the idea that under favorable meteorological conditions, high surface O_3 levels after sunlight hours could be sustained by continuous downmixing of free tropospheric air. The fact that nighttime O_3 could reach the same level as noontime O_3 is why previous studies suggested that physical transport was determining O_3 variations at NMC, while photochemistry played a minor role.

Diurnal variations of O_3 and PAN followed their averaged diel pattern on 72% and 75% out of the days with valid records, respectively. While O_3 diurnal cycles revealed more days with such daytime increases during summer (69% in spring vs. 74% in summer), PAN conformed better to its averaged diurnal cycle in spring (90% in spring vs. 63% in summer), suggesting that despite being under the same meteorological influences and despite highly similar average diurnal concentration profiles, O_3 and PAN often revealed different variations. O_3 and PAN increasing rates (on days with daytime increases) between 7:30 and 10:30 LT both displayed linear correlations to temperature increasing rates (Fig. S4), confirming again that their morning increases were closely connected to boundary layer development upon radiative heating. Prenoon (6:00 to 12:00 LT) O_3 concentrations also increased with PBLH during both spring (Fig. 5a) and summer (Fig. 5b), however, revealing slightly distinct slopes during distinct seasons. Weaker prenoon winds that mainly occurred during early morning under low PBLH conditions were associated with evidently lower O_3 concentrations. During early morning hours when PBLH was still low, strong winds that mostly came from the W-NW direction were associated with O_3 concentrations as high as those observed during noontime in the spring period (Fig. 5a). During the afternoon (12:00 to 18:00 LT), when the CBL has fully established, O_3 hardly displayed any more variation with PBLH (Fig. S5a), indicating that once boundary layer and free tropospheric air was fully mixed, O_3 did not further increase with PBLH. In the summer period, W-NW winds were less frequent and O_3 associated with these winds only increased weakly with PBLH, whereas N-NE winds resulted in more significant rise in O_3 over prenoon hours. Summertime afternoon PBLH was significantly lower than during spring due to frequent cloudy and rainy conditions, mostly falling into the range of 0.5-1.5 km (Fig. S5b). O_3 still increased with PBLH, however, revealing large variability under the same PBLH, indicating that PBLH was not the deterministic factor for afternoon O_3 levels. PAN did not replicate the variation of O_3 with PBLH during prenoon hours, displaying large variability at lower PBLH and moderate concentration levels under high PBLH. This suggests that free tropospheric O_3 levels were consistently and significantly higher than boundary layer O_3 levels, indicating for weak surface formation of O_3 (further discussed in Sect. 3.3), which resulted in significant increases in observed surface O_3 upon down mixing. Whereas free tropospheric PAN or the surface formation of PAN might have had higher variability, which resulted in largely different responses of PAN with the down mixing of free tropospheric air during afternoon hours.

https://doi.org/10.5194/egusphere-2023-182
Preprint. Discussion started: 29 March 2023

To investigate what has caused the discrepancies in free tropospheric O_3 and PAN over NMC, the variations of surface O_3 and PAN with free tropospheric (500-550 hPa) winds during spring and summer are depicted in Fig. 6. At lower wind speeds, both O_3 and PAN typically revealed lower concentrations. With increasing wind speeds, high concentrations of O_3 and PAN were associated with distinct wind directions, in both spring and summer. During springtime, high concentrations of O_3 and PAN both occurred with W winds, however, low O_3 and high PAN concentrations were detected under strong S winds. During summertime, high O_3 dominantly occurred with N-NE winds, while PAN mainly revealed elevated concentrations under S-SW winds. The distinct variation of O_3 and PAN with wind speed and wind direction suggests that the concentrations of both gases might have been impacted by different long-range transport processes, which will be investigated in the next section.

3.3 Impact of inter-regional transport and stratospheric-tropospheric exchange

Potential influence of pollution transport from India and other south Asian countries have been previously reported, which had potential impacts on the transport of PAN (Xu et al., 2018b). However, the source regions of O_3 and PAN in the TP have not been systematically investigated before. NO_2 and CO columns from TROPOMI revealed high concentrations in South Asian regions south of the TP contrasting to the pristine environment within the TP (Fig. 7). CO was more severe and widespread outside of the TP during the spring period, while NO_2 pollution was more severe during the summer period both in South Asia and to the east of the TP in China. Inside the TP, NO_2 and CO columns were both higher during the summer period, suggesting that summertime atmospheric circulations might have been more favorable for pollution transport into the TP. The high-altitude Himalaya mountains along the southern border of the TP is highly effective in blocking out direct intrusion of South Asian pollution, leading mostly to pollutant accumulation on its southern slope. High resolution satellite observations clearly reveal high NO_2 and CO along mountain and river valleys, indicating that pollution might have transported into the TP through these passageways. Belts of elevated CO extend from the western side (Kashmir) to the southeastern corner of the TP, indicating that pollution from South Asia could not directly cross over the Himalayas, especially not over those regions with very high altitudes, but had entered the TP by crossing either to its west or southeast.

To further identify possible source regions for high O_3 and PAN at NMC station, the PSCF for both gases were calculated for spring and summer, respectively (Fig. 8). Spring time high O_3 concentrations were mainly associated with westerly trajectories, which crossed over North India and Nepal before arriving at NMC (Fig. 8a). Although trajectories associated with high springtime O_3 crossed over vast areas outside the southern TP border, they mainly entered the TP from two passageways, one from the west and another from the southeast (near the border of Bhutan). Before entering the TP, the majority of the airmasses associated with high O_3 came from higher altitudes (> 6 km), diving downwards to heights of 3-6 km or even < 3 km near the southern border of the TP, and then entering the TP mainly from the west or south (Figs. 9a1-3). Aside from that, trajectories from the NW mostly travelling within 0-6 km (above ground level) were also associated with high springtime O_3. High springtime PAN, however, was only associated with trajectories crossing over South Asia and

https://doi.org/10.5194/egusphere-2023-182
Preprint. Discussion started: 29 March 2023

entering the TP from the southeastern border. In addition, airmasses from the Indian Ocean that travelled within 0-3 km and crossed over Bangladesh and Bhutan were also associated with high PAN, while not with high O_3 (Fig. 8b and Figs. 9b1-3). During summer, the PSCF of O_3 revealed a largely different distribution from that in spring. High altitude westerly airmasses that entered the TP from the west in spring have not been seen in summer, while airmasses sweeping along the southern border of the TP (Nepal and northern India) at altitudes below 6 km and approaching NMC from its south were still partly associated with high O_3 during summer (Fig. 8c and Figs. 9c1-3). Southerly low altitude (0-3 km) maritime airmasses that travelled over Bangladesh and Bhutan before entering the TP were also sometimes linked to high O_3 at NMC. However, the major summertime O_3 source regions were located to the north of NMC, including southern Xinjiang province, Northern Tibet and western Qinghai Province (Fig. 8c). High O_3 was mostly associated with low altitude airmasses from the NW and N directions (Fig. 9c1). Summertime PAN was only rarely associated with northerly airmasses, but mostly linked to westerly trajectories that travel along the southern TP border (mostly within 0-3 km, small parts within 3-6 km altitude, Figs. 9d1-2) and southerly trajectories travelling over Bangladesh and Bhutan within 3 km altitude (Fig. 9d1).

Thus, O_3 and PAN revealed distinct source regions in both spring and summer, while they also shared some common source regions. This explains why despite highly similar diel variation patterns, the day-to-day variation was often different between the two oxidants. Overall, springtime synoptic conditions resulted in a relatively monotone origin of airmasses at NMC, mostly favoring the subsidence of high altitude airmasses under westerly airflows, which were rich in both O_3 and PAN. With the onset of the South and East Asian Monsoon during summer, circulations drastically changed and resulted in influences of various distinct airmass origins at NMC. These vastly different airmass origins also exhibited completely different O_3 levels, with those originated in the north exhibiting even higher O_3 levels than those observed during springtime and southerly airmasses revealing much lower O_3 levels than during springtime. PAN, however, was more linked to westerly and southerly airmasses during summer.

Aside from changes in air mass origins at NMC, seasonal variations in large scale synoptic conditions were also deterministic of STE and the overall spatial distribution of O_3. Since the ERA5 reanalysis data has only considered simplified stratospheric O_3 chemistry and the physical transport of O_3, the O_3 mixing ratio in the ERA5 dataset is a good indicator for the investigation of stratospheric influences. During the spring period, the averaged ERA5 500 hPa O_3 revealed relatively lower mixing ratios in the TP region (especially in southeast TP) and higher mixing ratios outside the TP in the latitude band between 15 and 25°N. As was shown in previous studies, the downward transport of stratospheric O_3 and its distribution is closely linked to the location of the subtropical jet stream (Xu et al., 2018a) , which is typically located above the TP during the spring period (Fig. 10c1). Due to large scale circulations, lower stratospheric O_3 is typically high in polar regions, decreasing with latitude and reaching its lowest level in the equatorial belt (Fig. 10c1). Deep stratospheric intrusion and O_3 subsidence often occur along the lower edge of the subtropical jet stream, which is a slope extending from the lower stratosphere (150 hPa) between 38 to 42°N down to the middle or upper troposphere below 28°N. STE processes are especially promoted by fronts, which are accompanied by large scale subsidence of cold air from above (Stohl et al., 2003). STE mostly increased the O_3 levels in Southeast Asia to the west and south of the TP, which in turn could enhance O_3 at

https://doi.org/10.5194/egusphere-2023-182
Preprint. Discussion started: 29 March 2023

NMC through the westerly airmass transport passage (Figs. S6). Direct STE influence was also frequently observed during the spring period (on 5-8, 13, 23, 31 May and 3, 5 and 9 Jun, Figs. S7-13), with NMC frequently located near low pressure troughs behind cold fronts. These STE events were typically associated with high O_3 and low PAN concentrations, except for the 13 May, when stratospheric O_3 was transported to lower latitudes and then back to NMC via southwesterly winds, which also carried along high PAN concentrations, suggesting that NMC experienced aged stratospheric airmasses. During the summer period, with the northward shift of the subtropical jet stream, the high lower stratospheric O_3 concentrations were also confined within higher latitudes. 500 hPa ERA5 O_3 revealed a clearly distinct distribution from that during spring, displaying higher O_3 levels north of NMC (>30 °N) and much lower ones in the tropical region. Thus, under the prevailing southerly winds during the summer season, airmasses with lower stratospheric O_3 contents are transported to NMC. However, during two episodes on 7-9 and 21-25 Jul, northerly cold airmasses in front of 500 hPa high pressure systems over the TP brought stratospheric O_3 down to the norther TP regions and transported them within lower altitudes to NMC, resulting in surface O_3 levels even higher than those during springtime (Figs. S14-15), while PAN did not reveal significant increases. Statistically, $O_{3,ERA5}$ only explained 0.1% of the observed daytime O_3 day-to-day variability during spring (r=0.033), however, explained 22% of the summertime $O_{3,NMC}$ variability (r=0.47), contributing on average 10% during the entire observation period (Fig. S16), which was overall in accordance with previous results reported in Yin et al. (2017). It is also worth noting that observed O_3 at NMC was typically higher than the 550 hPa ERA5 O_3 mixing ratio, especially during spring and early summer (Fig. 10d). During the entire observation, stratospheric O_3 transport explained 83% of the observed daytime O_3 concentration ($O_{3,ERA5}/O_{3,NMC}$), with a lower contribution during spring (77%) and a higher one during summer (88%). This suggests that despite the small contributions of STE to the day-to-day variability of observed O_3, the overall daytime O_3 concentration was mainly maintained by the long-range transport of stratospheric O_3 (as opposed to direct strike of stratospheric O_3 during deep STE intrusions into the PBL). Additionally, the unexplained O_3 concentration might indicate for photochemical O_3 formation aside from pure physical transport. However, whether it was caused by local photochemical production or the long-range transport of photochemically produced O_3 still requires further investigation.

3.4 Impact of local photochemistry

As was already manifested, O_3 has its natural sources and is more affected by STE processes at high altitude locations such as NMC. O_3 is highly reactive and can be easily depleted in regions with high NO_x and VOCs emissions, however has a relatively longer lifetime in pristine background areas and can by directly or indirectly transported (transport of its precursors) over large distances, affecting O_3 levels at remote locations (Xu et al., 2018a). The impact of local photochemistry on the budget of O_3, however, was often under debate in previous studies conducted in background areas of the TP. Under such pristine atmospheric conditions, it was manifested that O_3 production was strongly NO_x-limited, with NO_x concentrations being the key factor determining whether O_3 was net produced or destructed in local photochemistry (Ma et al., 2002). However, the lower detection limit and precision of commercial instruments can hardly meet the needs for NO_x measurements in such clean environments, which made it difficult to determine whether there has been net O_3 formation. At

https://doi.org/10.5194/egusphere-2023-182
Preprint. Discussion started: 29 March 2023

higher altitudes, PAN has a long lifetime and can be transported over long distances. PAN measurements have been previously conducted at Mt. Waliguan (Northeastern TP) in 2006 (Xue et al., 2011) and at NMC station in the springs and summers of 2011 and 2012 (Xu et al., 2018b). At both sites, PAN contributed substantially to reactive nitrogen and acted as a good indicator for regional and long-range transport of polluted air plumes. The photochemical formation of PAN requires the presence of peroxyl acetyl radical and NO_2. The former is only formed in photochemical reactions of its precursor OVOCs, which are predominantly emitted within the boundary layer, while the latter is also mostly emitted near surface, with the exception of lightning processes. Altogether, the formation of PAN in comparison with O_3 is more favored near surface and has no natural sources. Nevertheless, the impact of local PAN formation versus those of transport to observed concentration levels was not discussed before due to the lack of its precursor measurements.

To evaluate the contribution of local photochemistry to observed O_3 and PAN, simulations were performed using an MCM-based box model for the period of 1 to 21 May, when VOCs measurements were available. Observed O_3 revealed much larger fluctuations than those obtained from all three simulation scenarios, which respectively used measurement constraints on OVOCs, NO_2 or both of them (Fig. 11a). With constraints on NO_2, modelling results revealed significant daytime increases, indicating positive local net photochemical formation of O_3 (Fig. 12a). However, when NO_2 was unconstrained, modelled O_3 concentrations were significantly lower and displayed very small variability, with very small positive net O_3 production during the morning and mostly negative ones during the day (Fig. 12a). Nevertheless, none of the simulations could reproduce the large variability and steep morning increases within observed O_3, with OVOCs and NO_2 both constrained by measurements, modelling results could only explain 28±19% (5-66%) of the observed daytime increases (Fig. 11b), while even less could be explained when only OVOCs or NO_2 was constrained (3±6% and 21±14%, respectively). Days with relatively stronger local photochemical O_3 formation were not necessary days with high observed O_3, while in return days with high O_3 were also often associated with weak photochemical net O_3 formation. This indicates that physical transport and mixing processes were determinative of O_3 diel cycle as well as the day-to-day O_3 variability, while local photochemistry further added to the daytime O_3 burden. Additionally, intercomparison among simulations also confirmed the high sensitivity of O_3 formation towards NO_x and the relatively weaker sensitivity to VOCs in such a pristine environment.

Simulated PAN levels under NO_2 constraints were, however, significantly higher than observed PAN concentrations, especially when OVOCs and NO_2 were both constrained. However, when NO_2 was unconstrained, PAN concentrations were mostly underestimated by simulations. Thermal decomposition of PAN was very weak under low springtime temperatures and net photochemical PAN formation rates were positive under all simulation scenarios, however, only NO_2 constrained cases revealed strong formation throughout daytime hours (08:00-20:00 LT) while unconstrained NO_2 simulations only displayed a very weak morning time (07:00-9:00 LT) photochemical formation. Only NO_2-constrained simulations overestimated PAN concentrations by a factor of 1.8 on average, however, could reproduce observed daytime PAN increments by 94±84%. Additionally, days with high simulated PAN photochemical production (4-6 and 13-17 May) corresponded to episodes with elevated observed PAN concentrations, which indicates that photochemical formation of PAN

https://doi.org/10.5194/egusphere-2023-182
Preprint. Discussion started: 29 March 2023

were determinative of its day-to-day variability. Compared to O_3, PAN was sensitive to concentrations of both OVOCs and NO_2, since some of the OVOCs are direct precursors of PA radicals, which combine with NO_2 in PAN formation. Still, NO_2 was more decisive of the overall O_3 and PAN production, since without its constraint, O_3 net loss and negligible PAN net formation would be yielded.

It should also be noted that both observed O_3 and PAN were not necessarily formed within the local boundary layer, since springtime winds in the TP are very strong, especially during daytime. Due to its relatively long lifetime, PAN might have been formed on the transport pathway to NMC, while O_3 might undergo both destruction and production during airmass transport. This might partly explain why PAN formation was overestimated by simulations representing surface conditions. But overall, it could be concluded that O_3 was mainly determined by physical transport, particularly STE processes, while PAN was largely determined by local photochemistry and that along the transport passageway. Fresh STE plumes reaching NMC from the north where PAN concentrations result in depleted surface PAN, while relatively aged STE airmasses crossing over polluted regions of Indo-Gigantic Plain led to simultaneous enrichment in surface O_3 and PAN. The high sensitivity of O_3 and PAN formation towards NO_x indicates that increased natural emission of NO_x under global warming, enhanced anthropogenic emissions of NO_x within the TP region due to the development of highways and transportation as well as increased transport input from South Asia might greatly enhance O_3 and PAN formation in background regions, while increased VOCs emissions and regional transport promotes PAN formation more than that of O_3.

4 Conclusions and implications

In this study, continuous measurements of O_3 and PAN as well as its precursors were conducted during spring and summer at a highly pristine high-altitude site in the southern TP (NMC station) to investigate the factors determining their variations. Due to the local topography, surface observations at NMC reflects free tropospheric air conditions during daytime and nocturnal boundary layer conditions during nighttime. Both O_3 and PAN revealed steep increases after sunrise and reached a flat plateau during daytime. While averaged diurnal variations of O_3 and PAN highly resembled each other, their day-to-day variations were often different, suggesting that they might have been influenced by distinct physiochemical processes.

Backward trajectory modelling and PSCF analysis revealed distinct source regions connected to high O_3 and PAN. During spring, airmasses rich in O_3 were mainly associated with high altitude westerly airmasses that either entered the TP from the west of from the south, while PAN was only rich in westerly airmasses that transported along the polluted regions in North India and Nepal before entering the TP from the south or in southerly maritime airmasses that crossed over polluted South Asian regions before entering the TP. During the summer monsoon season, airmasses from the north were associated with the highest O_3 levels, while westerly and southerly airmasses revealed lower O_3 levels. Elevated PAN concentrations, however, were still linked to westerly and southerly airmasses crossing over polluted South Asian regions. O_3 at NMC was strongly influenced by STE, which brought down high stratospheric O_3 concentrations from the southwest route during spring and from the northwest during summer, explaining 77% and 88% of the observed O_3 level in spring and summer,

https://doi.org/10.5194/egusphere-2023-182
Preprint. Discussion started: 29 March 2023

respectively. PAN concentrations were, however, typically lower in airmasses with strong stratospheric influence, except if they transported over polluted regions south of the TP.

Photochemistry resulted in positive net formation of both O_3 and PAN. While only 28±19% of the observed daytime growth in O_3 could be explained by photochemical simulations, the daytime growth of PAN was highly overestimated by the model if OVOCs and NO_2 were both constrained. Photochemistry was not the factor determining the day-to-day variability of O_3, however, explained observed PAN variabilities well. While both O_3 and PAN formation were highly sensitive to NO_x levels, PAN was also quite sensitive to VOCs concentrations. Therefore, future concentrations of O_3 and PAN over the TP may be significantly impacted by increases in the concentrations of NO_x, VOCs, and other precursors, which either originate from the surrounding regions (in particular South Asia) or from anthropogenic and natural sources within the TP. Special attention should be addressed to PAN, which is mostly determined by photochemical processes sensitive to both NO_x and VOCs and can be transported over very long distances.

Data availability. The data used in this study are available on the @Tibet ftp server (http://at-tibet.quickconnect.cn/) and can be applied for upon request to the corresponding authors (zhanggen@cma.gov.cn and c.ye@pku.edu.cn)

Author contributions. WX and CY designed the experiment and led the research. WX, GZ, CY, YW, YZ, YB, WL, XX were responsible for the maintenance of trace gas and meteorology measurements in the experiment and WX, YZ and YW processed the data. WX analyzed the data and wrote the paper with help from XZ, XX and GZ.

Competing interests. The authors declare that they have no conflict of interest.

Acknowledgments, Samples, and Data

This work is supported by the National Natural Science Foundation of China (41875159, 42175127, 42275127, 42075112, and 42105110) and the Natural Science Foundation of Beijing (8222078).

References

Ara Begum, B., Kim, E., Jeong, C.-H., Lee, D.-W., and Hopke, P. K.: Evaluation of the potential source contribution function using the 2002 Quebec forest fire episode, Atmospheric Environment, 39, 3719-3724, 10.1016/j.atmosenv.2005.03.008, 2005.
Ding, A., and Wang, T.: Influence of stratosphere-to-troposphere exchange on the seasonal cycle of surface ozone at Mount Waliguan in western China, Geophysical Research Letters, 33, L03803, 10.1029/2005GL024760, 2006.
Draxler, R. R., and Hess, G. D.: Description of the HYSPLIT_4 modeling system, NOAA Tech. Memo, ERL ARL-224, NOAA Air Resources Laboratory, Silver Spring, MD, 24 pp., 1997.
Draxler, R. R., and Hess, G. D.: An overview of the HYSPLIT_4 modelling system for trajectories, dispersion and deposition, Australian Meteorological Magazine, 47, 295-308, 1998.
Draxler, R. R.: HYSPLIT4 user's guide, NOAA Tech. Memo, ERL ARL-230, NOAA Air Resources Laboratory, Silver Spring, MD, 1999.

https://doi.org/10.5194/egusphere-2023-182
Preprint. Discussion started: 29 March 2023

Fischer, E. V., Jacob, D. J., Yantosca, R. M., Sulprizio, M. P., Millet, D. B., Mao, J., Paulot, F., Singh, H. B., Roiger, A., Ries, L., Talbot, R. W., Dzepina, K., and Pandey Deolal, S.: Atmospheric peroxyacetyl nitrate (PAN): a global budget and source attribution, Atmos. Chem. Phys., 14, 2679-2698, 10.5194/acp-14-2679-2014, 2014.
Hu, B., Liu, T., Hong, Y., Xu, L., Li, M., Wu, X., Wang, H., Chen, J., and Chen, J.: Characteristics of peroxyacetyl nitrate (PAN) in a coastal city of southeastern China: Photochemical mechanism and pollution process, Science of The Total Environment, 719, 137493, https://doi.org/10.1016/j.scitotenv.2020.137493, 2020.
Kleindienst, T. E., Shepson, P. B., and Smith, D. F.: Comparison of mutagenic activities of several peroxyacyl nitrates, Environmental and molecular mutagenesis, 16, 70-80, 1990.
Langford, A. O.: Stratosphere-troposphere exchange at the subtropical jet: Contribution to the tropospheric ozone budget at midlatitudes, Geophysical Research Letters, 26, 2449-2452, 10.1029/1999GL900556, 1999.
Lefohn, A. S., Malley, C. S., Simon, H., Wells, B., Xu, X., Zhang, L., and Wang, T.: Responses of human health and vegetation exposure metrics to changes in ozone concentration distributions in the European Union, United States, and China, Atmospheric Environment, 152, 123-145, https://doi.org/10.1016/j.atmosenv.2016.12.025, 2017.
Lin, W., Xu, X., Zheng, X., Dawa, J., Baima, C., and Ma, J.: Two-year measurements of surface ozone at Dangxiong, a remote highland site in the Tibetan Plateau, Journal of Environmental Sciences, 31, 133-145, http://dx.doi.org/10.1016/j.jes.2014.10.022, 2015.
Liu, L., Wang, X., Chen, J., Xue, L., Wang, W., Wen, L., Li, D., and Chen, T.: Understanding unusually high levels of peroxyacetyl nitrate (PAN) in winter in Urban Jinan, China, Journal of Environmental Sciences, 71, 249-260, https://doi.org/10.1016/j.jes.2018.05.015, 2018.
Lucey, D., Hadjiiski, L., Hopke, P. K., Scudlark, J. R., and Church, T.: Identification of sources of pollutants in precipitation measured at the mid-Atlantic US coast using potential source contribution function (PSCF), Atmospheric Environment, 35, 3979-3986, 10.1016/s1352-2310(01)00185-6, 2001.
Ma, J., Tang, J., Zhou, X., and Zhang, X.: Estimates of the Chemical Budget for Ozone at Waliguan Observatory, Journal of Atmospheric Chemistry, 41, 21-48, 10.1023/A:1013892308983, 2002.
Ma, J., Lin, W. L., Zheng, X. D., Xu, X. B., Li, Z., and Yang, L. L.: Influence of air mass downward transport on the variability of surface ozone at Xianggelila Regional Atmosphere Background Station, southwest China, Atmospheric Chemistry and Physics, 14, 5311-5325, 10.5194/acp-14-5311-2014, 2014.
Moxim, W. J., Levy, H., II, and Kasibhatla, P. S.: Simulated global tropospheric PAN: Its transport and impact on NOx, J. Geophys. Res., 101, 12621-12638, 10.1029/96jd00338, 1996.
Qiu, Y., Ma, Z., Li, K., Huang, M., Sheng, J., Tian, P., Zhu, J., Pu, W., Tang, Y., Han, T., Zhou, H., and Liao, H.: Measurement report: Fast photochemical production of peroxyacetyl nitrate (PAN) over the rural North China Plain during haze events in autumn, Atmos. Chem. Phys., 21, 17995-18010, 10.5194/acp-21-17995-2021, 2021.
Singh, H. B., and Hanst, P. L.: Peroxyacetyl nitrate (PAN) in the unpolluted atmosphere: An important reservoir for nitrogen oxides, Geophysical Research Letters, 8, 941-944, 10.1029/GL008i008p00941, 1981.
Škerlak, B., Sprenger, M., and Wernli, H.: A global climatology of stratosphere–troposphere exchange using the ERA-Interim data set from 1979 to 2011, Atmospheric Chemistry and Physics, 14, 913-937, 10.5194/acp-14-913-2014, 2014.
Sprenger, M., and Wernli, H.: A northern hemispheric climatology of cross-tropopause exchange for the ERA15 time period (1979–1993), Journal of Geophysical Research: Atmospheres, 108, 8521, 10.1029/2002JD002636, 2003.
Sprenger, M., Wernli, H., and Bourqui, M.: Stratosphere–Troposphere Exchange and Its Relation to Potential Vorticity Streamers and Cutoffs near the Extratropical Tropopause, Journal of the Atmospheric Sciences, 64, 1587-1602, 10.1175/jas3911.1, 2007.
Stohl, A., Bonasoni, P., Cristofanelli, P., Collins, W., Feichter, J., Frank, A., Forster, C., Gerasopoulos, E., Gäggeler, H., James, P., Kentarchos, T., Kromp-Kolb, H., Krüger, B., Land, C., Meloen, J., Papayannis, A., Priller, A., Seibert, P., Sprenger, M., Roelofs, G. J., Scheel, H. E., Schnabel, C., Siegmund, P., Tobler, L., Trickl, T., Wernli, H., Wirth, V., Zanis, P., and Zerefos, C.: Stratosphere-troposphere exchange: A review, and what we have learned from STACCATO, Journal of Geophysical Research: Atmospheres, 108, 8516, 10.1029/2002JD002490, 2003.
Tang, Q., Prather, M. J., and Hsu, J.: Stratosphere-troposphere exchange ozone flux related to deep convection, Geophysical Research Letters, 38, L03806, 10.1029/2010gl046039, 2011.
Taylor, O.: Importance of peroxyacetyl nitrate (PAN) as a phytotoxic air pollutant, Journal of the Air Pollution Control Association, 19, 347-351, 1969.
Wei, W., Zang, J., Wang, X., and Cheng, S.: Peroxyacetyl nitrate (PAN) in the border of Beijing, Tianjin and Hebei of China: Concentration, source apportionment and photochemical pollution assessment, Atmospheric Research, 246, 105106, https://doi.org/10.1016/j.atmosres.2020.105106, 2020.
Wolfe, G. M., Marvin, M. R., Roberts, S. J., Travis, K. R., and Liao, J.: The Framework for 0-D Atmospheric Modeling (F0AM) v3.1, Geosci. Model Dev., 9, 3309-3319, 10.5194/gmd-9-3309-2016, 2016.
Xu, W., Lin, W., Xu, X., Tang, J., Huang, J., Wu, H., and Zhang, X.: Long-term trends of surface ozone and its influencing factors at the Mt Waliguan GAW station, China – Part 1: Overall trends and characteristics, Atmospheric Chemistry and Physics, 16, 6191-6205, 10.5194/acp-16-6191-2016, 2016.

https://doi.org/10.5194/egusphere-2023-182
Preprint. Discussion started: 29 March 2023

Xu, W., Xu, X., Lin, M., Lin, W., Tarasick, D., Tang, J., Ma, J., and Zheng, X.: Long-term trends of surface ozone and its influencing factors at the Mt Waliguan GAW station, China – Part 2: The roles of anthropogenic emissions and climate variability, Atmos. Chem. Phys., 18, 773-798, 10.5194/acp-18-773-2018, 2018a.

Xu, W., Zhang, G., Wang, Y., Tong, S., Zhang, W., Ma, Z., Lin, W., Kuang, Y., Yin, L., and Xu, X.: Aerosol Promotes Peroxyacetyl Nitrate Formation During Winter in the North China Plain, Environmental Science & Technology, 55, 3568-3581, 10.1021/acs.est.0c08157, 2021.

Xu, X., Zhang, H., Lin, W., Wang, Y., Xu, W., and Jia, S.: First simultaneous measurements of peroxyacetyl nitrate (PAN) and ozone at Nam Co in the central Tibetan Plateau: impacts from the PBL evolution and transport processes, Atmos. Chem. Phys., 18, 5199-5217, 10.5194/acp-18-5199-2018, 2018b.

Xue, L. K., Wang, T., Zhang, J. M., Zhang, X. C., Deliger, Poon, C. N., Ding, A. J., Zhou, X. H., Wu, W. S., Tang, J., Zhang, Q. Z., and Wang, W. X.: Source of surface ozone and reactive nitrogen speciation at Mount Waliguan in western China: New insights from the 2006 summer study, Jounal of Geophysical Research, 116, D07306, 10.1029/2010jd014735, 2011.

Xue, L. K., Wang, T., Guo, H., Blake, D. R., Tang, J., Zhang, X. C., Saunders, S. M., and Wang, W. X.: Sources and photochemistry of volatile organic compounds in the remote atmosphere of western China: results from the Mt. Waliguan Observatory, Atmos. Chem. Phys., 13, 8551-8567, 10.5194/acp-13-8551-2013, 2013.

Yang, K., Wu, H., Qin, J., Lin, C., Tang, W., and Chen, Y.: Recent climate changes over the Tibetan Plateau and their impacts on energy and water cycle: A review, Global and Planetary Change, 112, 79-91, https://doi.org/10.1016/j.gloplacha.2013.12.001, 2014.

Yao, Q., Ma, Z., Lin, W., Liu, J.-l., Wang, X., Cai, Z., and Han, S.: Transport Characteristics of PAN and O3 in the Lower Atmosphere of the Boundary Layer in Tianjin in Summer, environmental science, 40, 67-75, 10.13227 /j.hjkx.201805070, 2019.

Yin, X., Kang, S., de Foy, B., Cong, Z., Luo, J., Zhang, L., Ma, Y., Zhang, G., Rupakheti, D., and Zhang, Q.: Surface ozone at Nam Co in the inland Tibetan Plateau: variation, synthesis comparison and regional representativeness, Atmos. Chem. Phys., 17, 11293-11311, 10.5194/acp-17-11293-2017, 2017.

Yukihiro, M., Hiramatsu, T., Bouteau, F., Kadono, T., and Kawano, T.: Peroxyacetyl nitrate-induced oxidative and calcium signaling events leading to cell death in ozone-sensitive tobacco cell-line, Plant Signaling & Behavior, 7, 113-120, 10.4161/psb.7.1.18376, 2012.

Zeng, Y., and Hopke, P. K.: A studyof the sources of acid precipitation in Ontario, Canada, Atmospheric Environment, 23, 1499-1509, 1989.

Zhang, G., Xia, L., Zang, K., Xu, W., Zhang, F., Liang, L., Yao, B., Lin, W., and Mu, Y.: The abundance and inter-relationship of atmospheric peroxyacetyl nitrate (PAN), peroxypropionyl nitrate (PPN), O3, and NOy during the wintertime in Beijing, China, Science of The Total Environment, 718, 137388, https://doi.org/10.1016/j.scitotenv.2020.137388, 2020.

Zhang, G., Jing, S., Xu, W., Gao, Y., Yan, C., Liang, L., Huang, C., and Wang, H.: Simultaneous observation of atmospheric peroxyacetyl nitrate and ozone in the megacity of Shanghai, China: Regional transport and thermal decomposition, Environmental Pollution, 274, 116570, https://doi.org/10.1016/j.envpol.2021.116570, 2021.

Zhang, J. M., Wang, T., Ding, A. J., Zhou, X. H., Xue, L. K., Poon, C. N., Wu, W. S., Gao, J., Zuo, H. C., Chen, J. M., Zhang, X. C., and Fan, S. J.: Continuous measurement of peroxyacetyl nitrate (PAN) in suburban and remote areas of western China, Atmospheric Environment, 43, 228-237, 10.1016/j.atmosenv.2008.09.070, 2009.

Zheng, X., Wan, G., Chen, Z., and Tang, J.: Measurement and meteorological analysis of 7Be and 210Pb in aerosol at Waliguan Observatory, Advances in Atmospheric Sciences, 25, 404-416, 10.1007/s00376-008-0404-y, 2008.

Zhou, L., Hopke, P. K., and Liu, W.: Comparison of two trajectory based models for locating particle sources for two rural New York sites, Atmospheric Environment, 38, 1955-1963, 10.1016/j.atmosenv.2003.12.034, 2004.

https://doi.org/10.5194/egusphere-2023-182
Preprint. Discussion started: 29 March 2023

583 **Table 1** Statistics of trace gases (including O_3, PAN, NO_2, CO, OVOCs, aromatics, alkanes and alkenes), photolysis rates (jO^1D and jNO_2),
584 meteorological variables, as well as the Y index

Variable	Unit	Spring			Summer		
		all	day (8:00-20:00)	night (20:00-8:00)	all	day	night
O_3	ppb	59.8±13.4	67.8±9.0	52.2±12.4	53.6±13.2	58.3±12.5	48.8±12.1
PAN	ppb	0.27±0.08	0.30±0.07	0.24±0.07	0.20±0.05	0.21±0.05	0.18±0.05
NO_2	ppb	0.12±0.05	0.11±0.07	0.13±0.04	0.09±0.05	0.08±0.03	0.10±0.06
CO	ppb	108±26	108±16	107±33	117±29	116±33	118±24
CH_4	ppm	1.890±0.024	1.884±0.012	1.895±0.030	1.886±0.021	1.883±0.017	1.887±0.024
OVOCs		2.49±2.16	3.10±2.60	1.88±1.34		-	-
Aromatics	Propy-Equiv. ppbC	0.56±1.29	0.61±1.74	0.51±0.55	-	-	-
Alkanes		0.47±0.50	0.48±0.59	0.46±0.40	-	-	-
Alkenes		0.59±0.57	0.71±0.68	0.47±0.39	-	-	-
jO^1D	10^{-7} s^{-1}	-	277±183	-	-	275	-
jNO_2	10^{-4} s^{-1}	-	70±27	-	-	66±29	-
Temperature	°C	4.2±4.1	6.6±3.4	2.0±3.5	9.3±3.5	10.9±3.5	7.7±2.8
RH	%	50±19	41±18	59±17	61±19	55±19	68±17
Cumulated Rain	mm	1.0	0.8	0.2	37.3	24.1	13.2
Wind Speed	m s^{-1}	4.0±2.6	4.8±2.3	3.3±2.6	3.9±2.3	4.2±2.2	3.6±2.4
Y index	-	1.7±0.9	2.1±0.9	1.4±0.6	0.8±0.3	0.9±0.4	0.7±0.3

585

https://doi.org/10.5194/egusphere-2023-182
Preprint. Discussion started: 29 March 2023

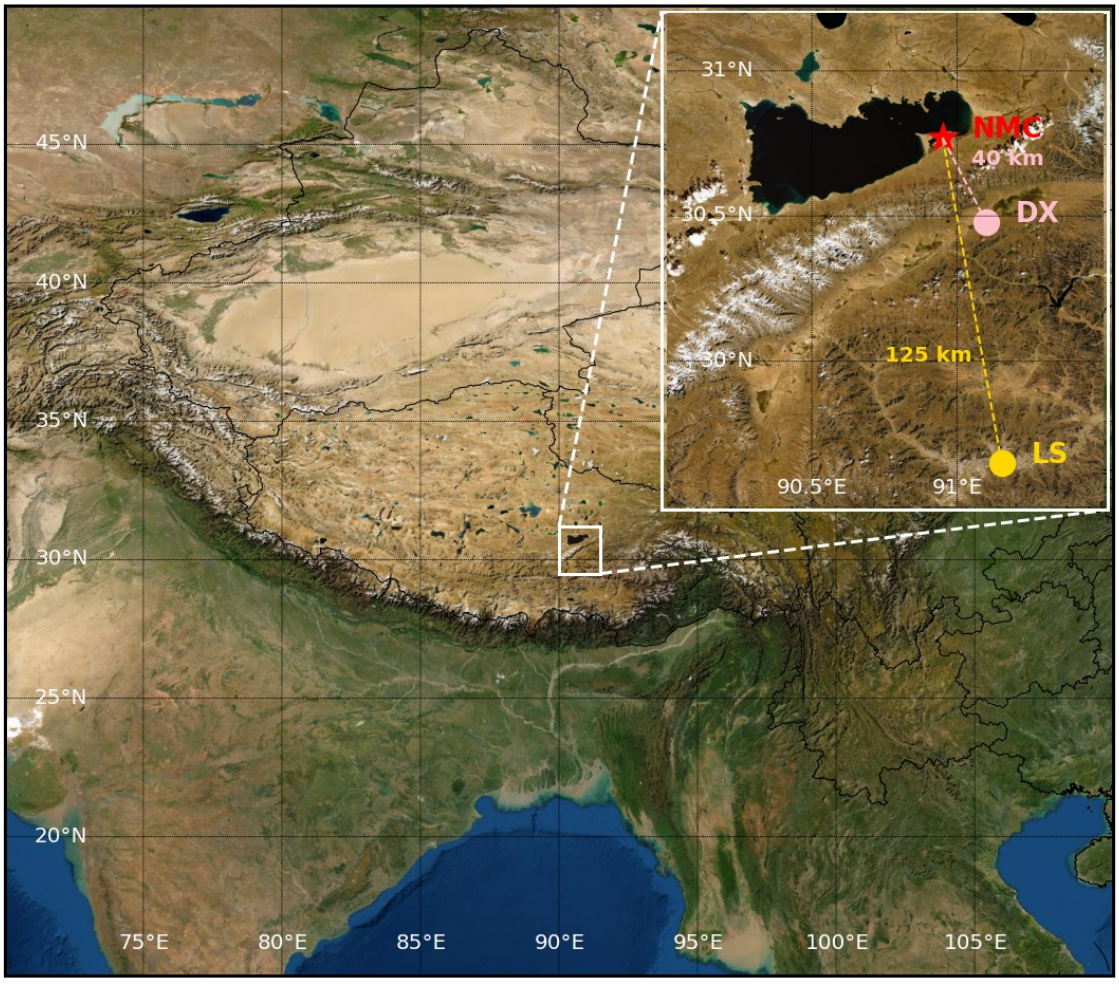

586

587 **Figure 1. Map displaying the locations of the Nam Co site (NMC), Dangxiong (DX) county and Lhasa city (LS). This figure was**
588 **draw based on Map service in ArcGIS World Imagery (https://doc.arcgis.com/en/data-appliance/6.4/maps/world-imagery.htm)**

589

https://doi.org/10.5194/egusphere-2023-182
Preprint. Discussion started: 29 March 2023

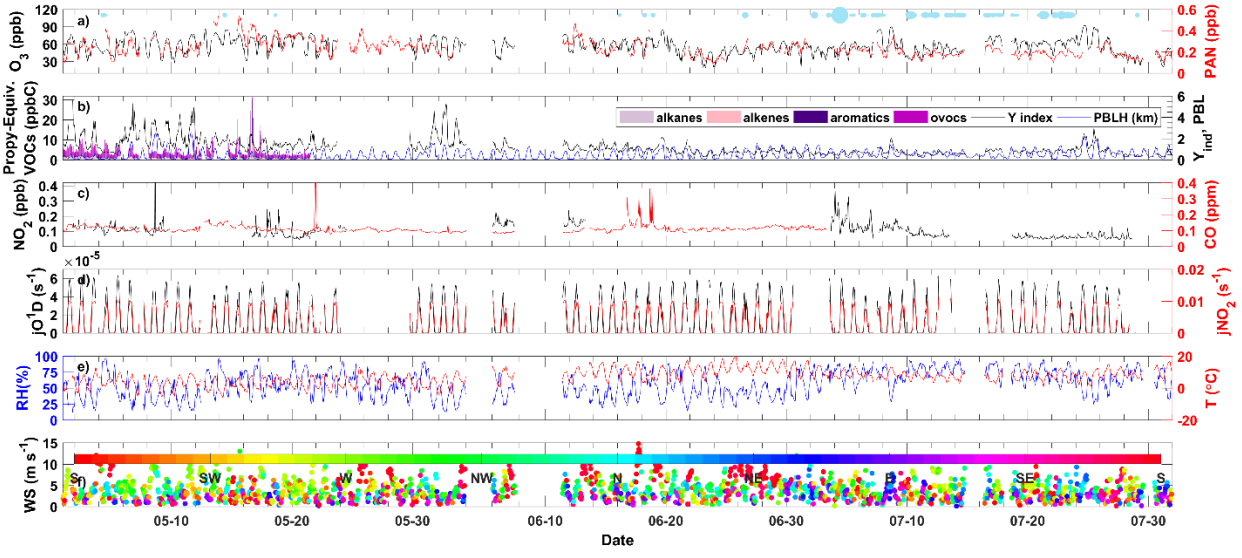

Figure 2 Timeseries of a) O_3, PAN, b) NO_2, CO, c) jO^1D, jNO_2, d) RH, T, e) wind speed and wind direction during the Nam Co campaign from 1 May to 31 Jul.

https://doi.org/10.5194/egusphere-2023-182
Preprint. Discussion started: 29 March 2023

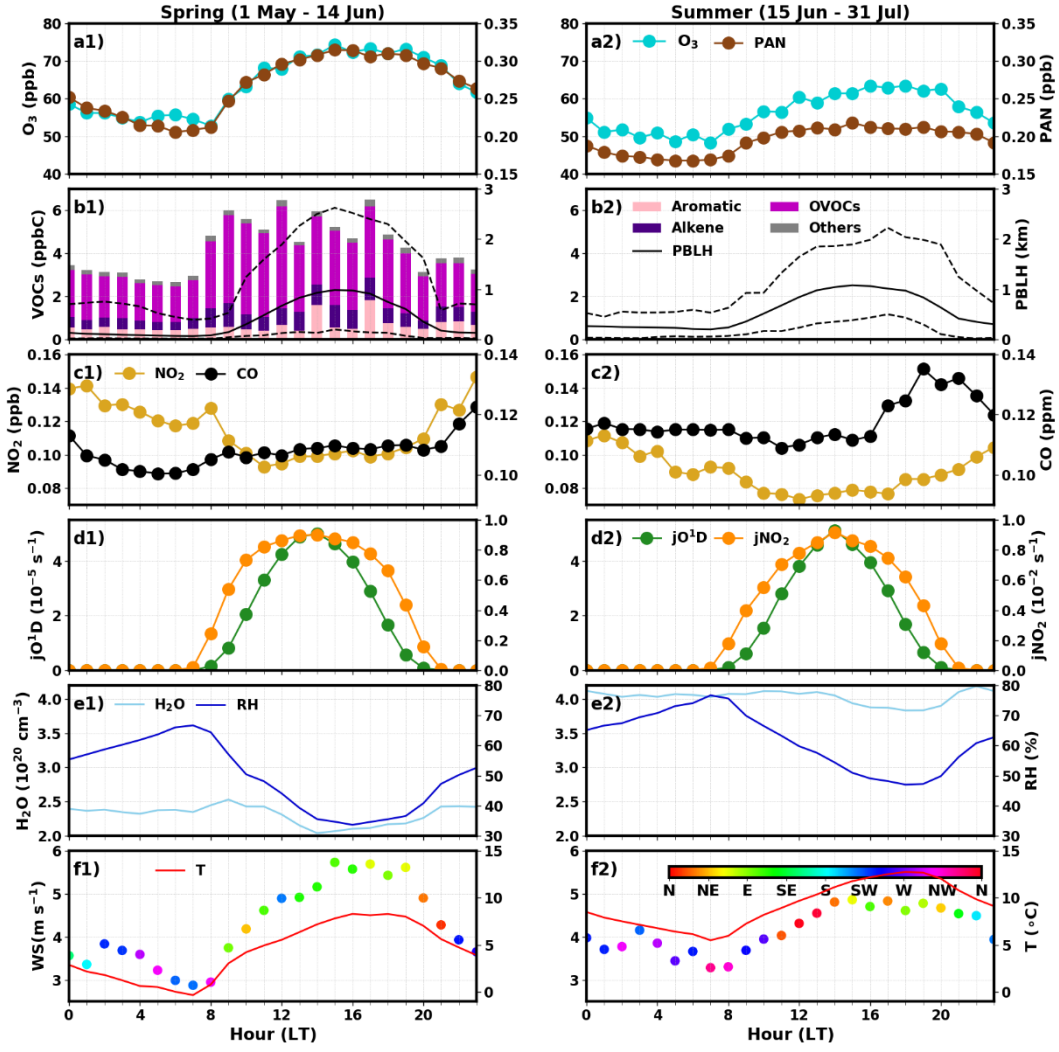

Figure 3. Averaged diurnal variations of a) O_3, PAN, b) VOCs, PBLH (solid line black line: average value, dashed black lines: minimum and maximum value) c) NO_2, CO, d) jO^1D, jNO_2, e) H_2O, RH and f) temperature, wind speed and wind direction during the 1) spring and 2) summer period, respectively.

https://doi.org/10.5194/egusphere-2023-182
Preprint. Discussion started: 29 March 2023

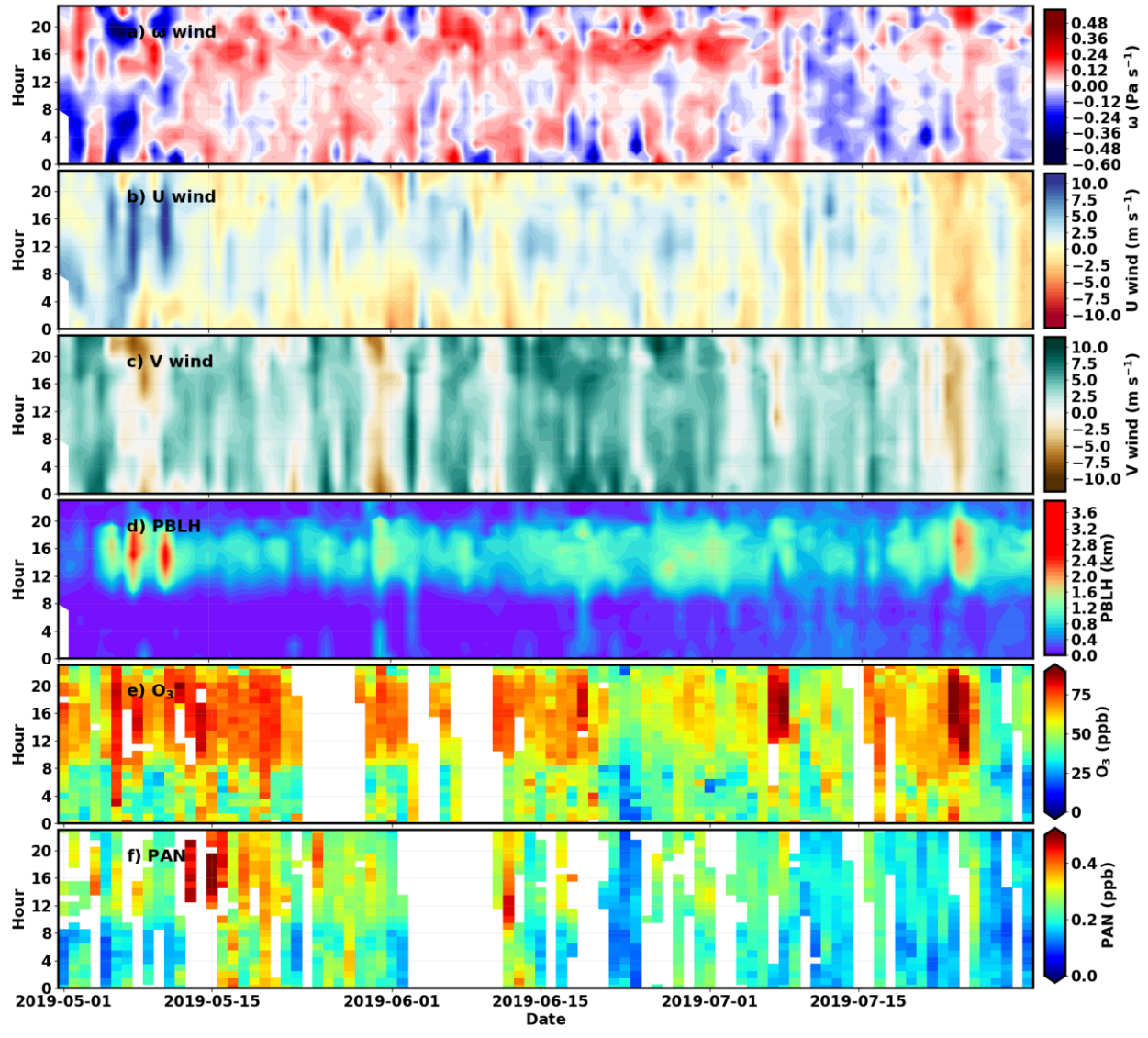

Figure 4. Season-diurnal variations of a) ω wind, b) U wind, c) V wind, d) PBLH, e) surface O_3 and f) PAN between 1 May and 31 Jul 2019 at Nam Co.

https://doi.org/10.5194/egusphere-2023-182
Preprint. Discussion started: 29 March 2023

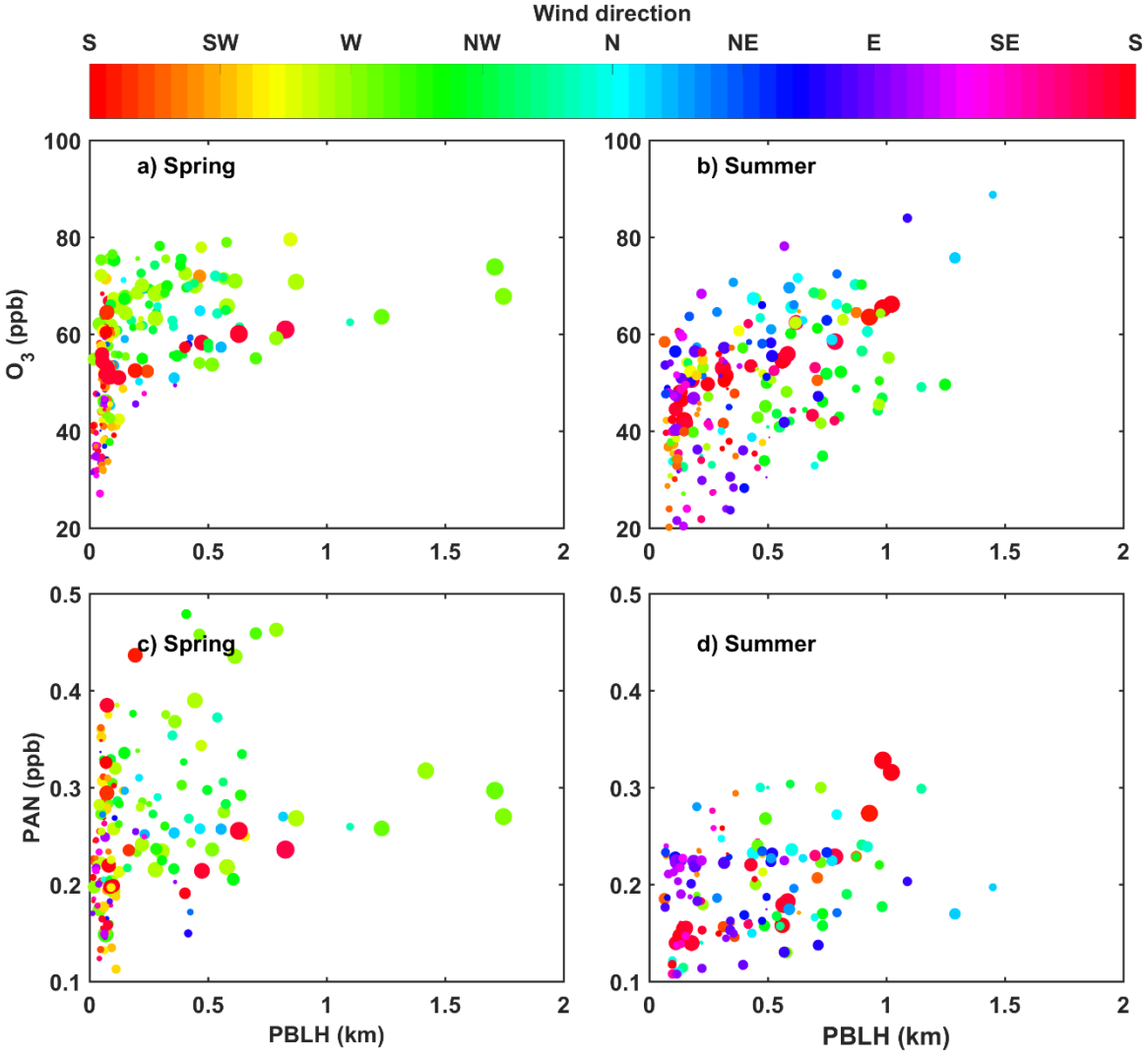

603

604 **Figure 5. Variation of prenoon (6:00-12:00) O_3 (a,b) and PAN (c,d) with PBLH (from ERA5 reanalysis data) during spring (a,c)**
605 **and summer (b,d) periods, with wind speeds and directions indicated by sizes and colors of scattered dots (precipitation associated**
606 **data points excluded).**

607

https://doi.org/10.5194/egusphere-2023-182
Preprint. Discussion started: 29 March 2023

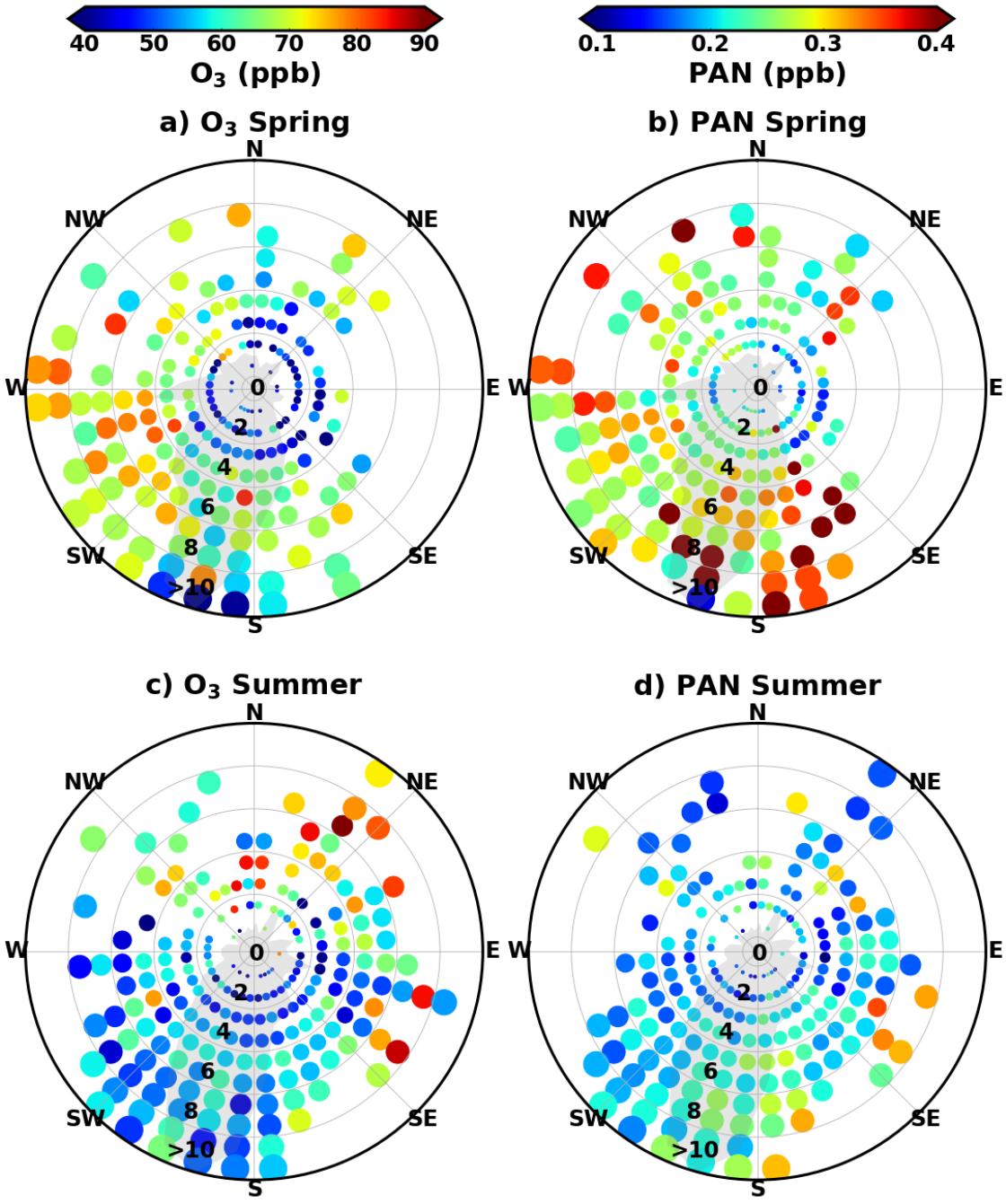

608

609 **Figure 6. Variation of springtime (a,b) and summertime (c,d) O_3 (a,c) and PAN (b,d) concentrations with 2m wind speeds and 500-**
610 **550 hPa wind directions from ECMWF ERA5 data. Gray shading represents the relative occurrence frequency of wind directions.**

611

https://doi.org/10.5194/egusphere-2023-182
Preprint. Discussion started: 29 March 2023

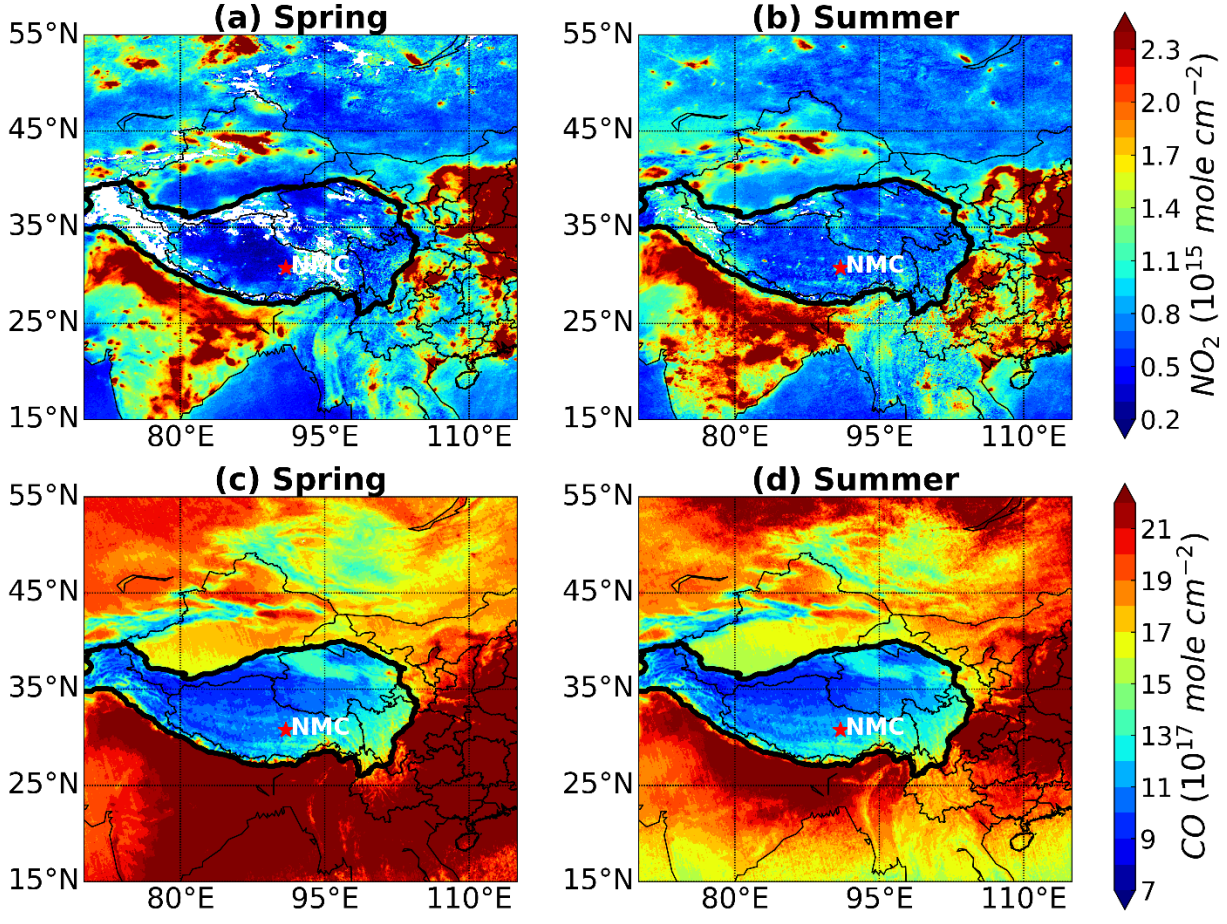

612

613 **Figure 7. TROPOMI NO_2 (a,b) and CO (c,d) column concentration distributions averaged over spring (a,c) and summer (b,d)**
614 **periods.**

615

https://doi.org/10.5194/egusphere-2023-182
Preprint. Discussion started: 29 March 2023

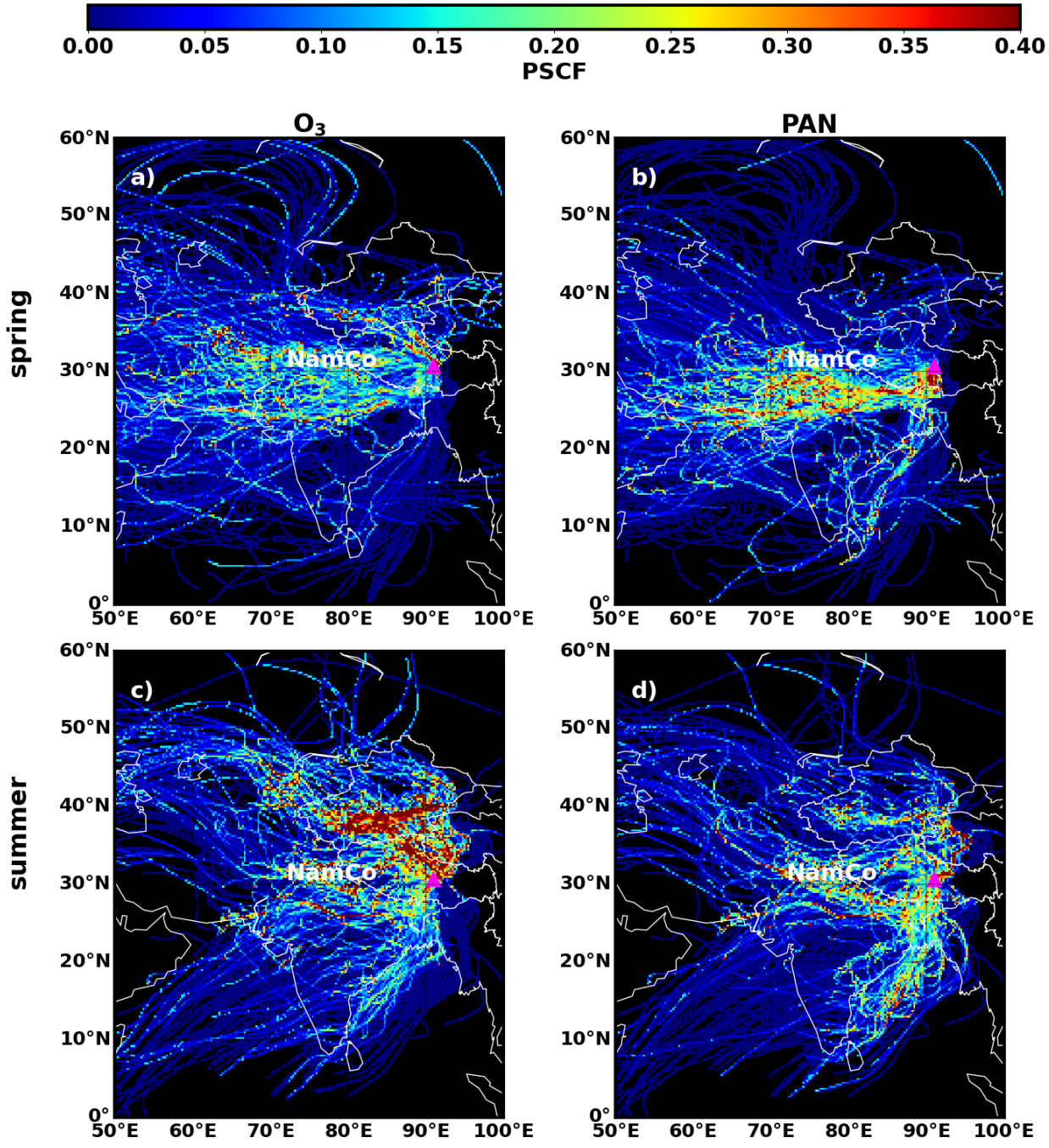

616

617 **Figure 8. Potential Source Contribution Function (PSCF) of O_3 (a,c) and PAN (b,d) during spring (a,b) and summer (c,d) periods.**

618

https://doi.org/10.5194/egusphere-2023-182
Preprint. Discussion started: 29 March 2023

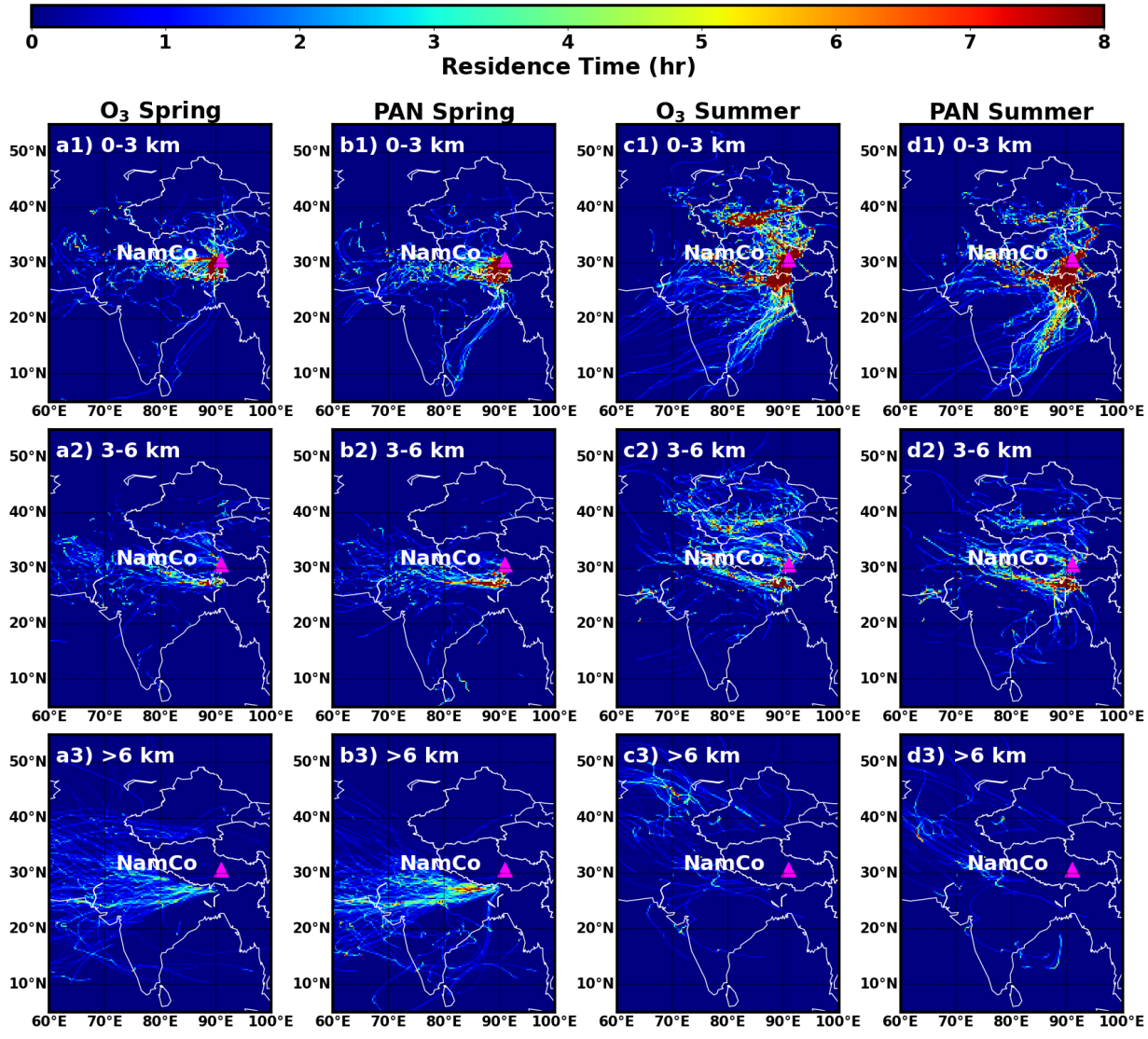

619

620 **Figure 9. Residence time of trajectories associated with O_3 (a,c) and PAN (b,d) above their respective 67th percentiles during spring**
621 **(a,b) and summer (c,d) periods within height ranges (above ground level) of 1) 0-3 km, 2) 3-6 km and 3) >6 km.**

622

https://doi.org/10.5194/egusphere-2023-182
Preprint. Discussion started: 29 March 2023

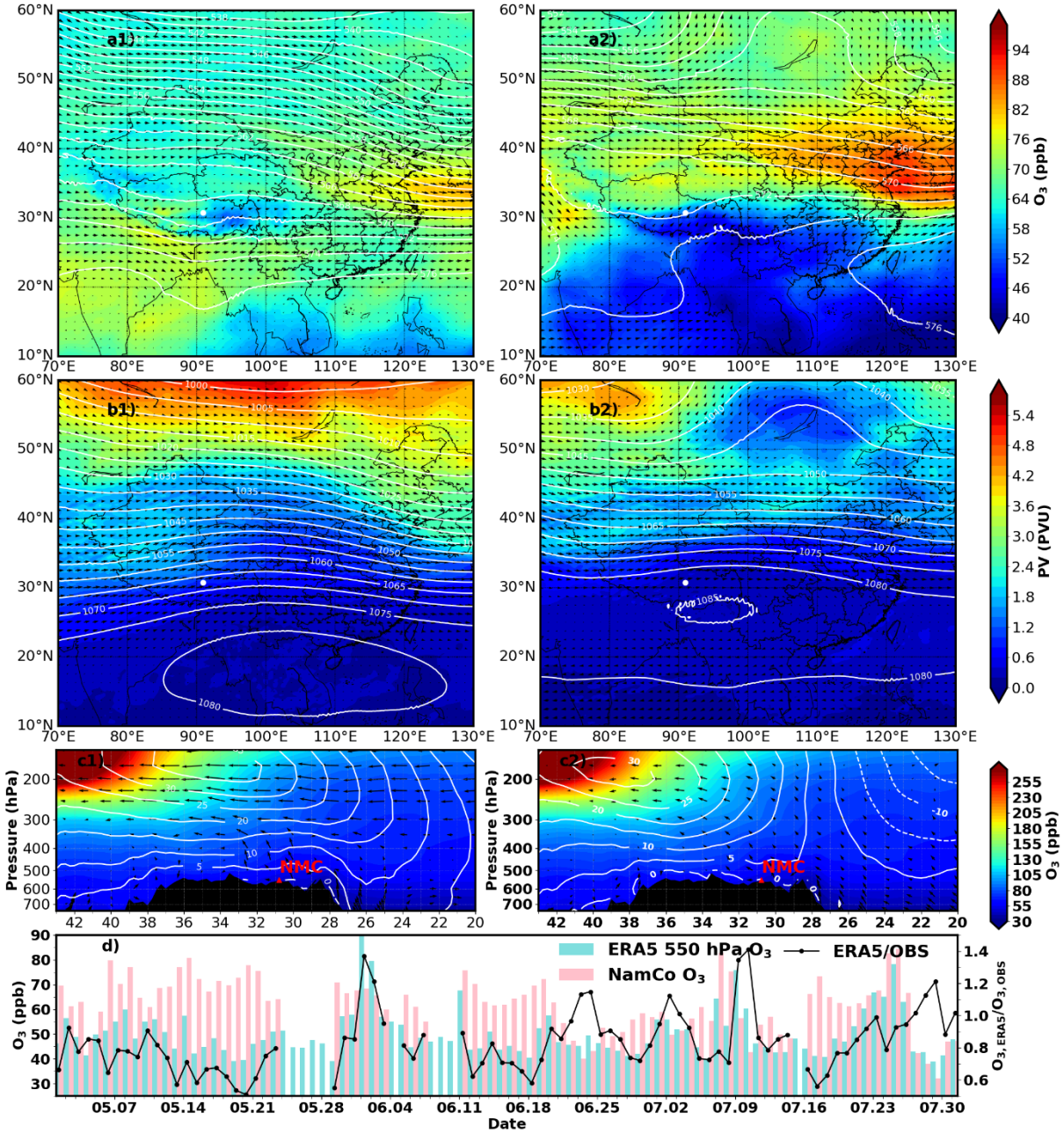

Figure 10. Distribution of a) ERA5 500 hPa O_3 mixing ratio, geopotential height (white contour lines) and winds (black arrows), b) 250 hPa potential vorticity, geopotential height and winds, c) cross-section of O_3 mixing ratio, u winds (white contour lines), v winds and vertical velocity (black arrows) at the longitude of Nam Co station and d) the comparison between daytime ERA5 550 hPa and observed O_3 mixing ratio at Nam Co.

https://doi.org/10.5194/egusphere-2023-182
Preprint. Discussion started: 29 March 2023

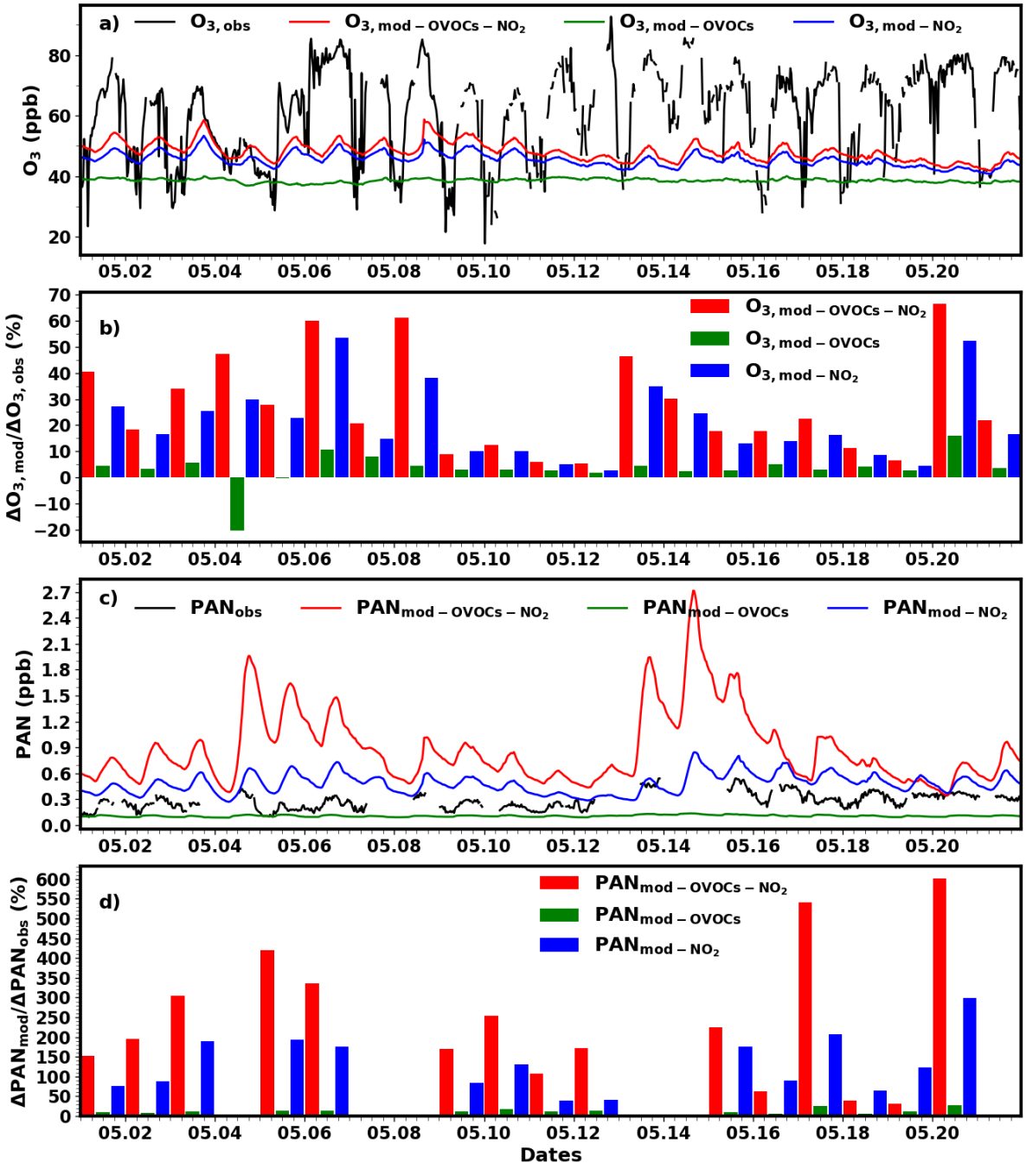

Figure 11. a) Observed (black) and modelled O_3 using constraints on OVOCs (green), NO_2 (blue) and both (red), b) percentage of observed daytime O_3 concentration increment ($\Delta O_{3,obs}$) that can be explained by those modelled under different constraints ($\Delta O_{3,mod}$), c) observed (black) and modelled PAN under OVOCs (green), NO_2(blue) and both constraints (red), d) percentage of observed daytime PAN concentration increment (ΔPAN_{obs}) that can be explained by those modelled under different constraints (ΔPAN_{mod}).

https://doi.org/10.5194/egusphere-2023-182
Preprint. Discussion started: 29 March 2023

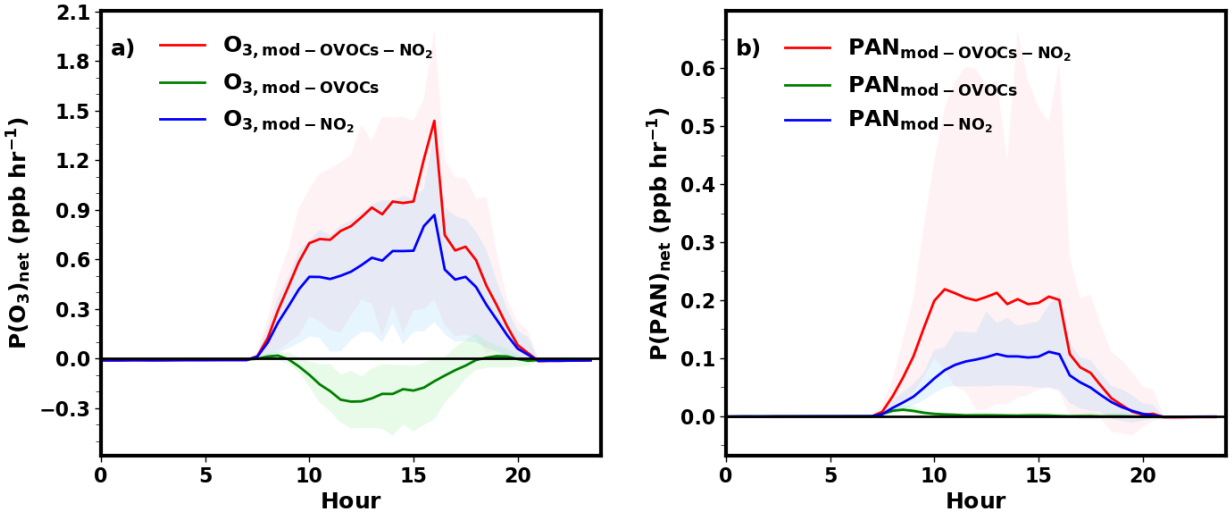

Figure 12. Net production rate of a) O_3 and b) PAN simulated under OVOCs (green), NO_2 (blue) and OVOCs+NO_2 combined measurement constraints. Shaded areas represent calculated ranges of 5^{th} to 95^{th} percentiles.